Monte Carlo Simulations of Supercoiled DNAs Confined to a Plane

Bryant S. Fujimoto and J. Michael Schurr
Department of Chemistry, University of Washington, Seattle, Washington 98195-1700 USA

ABSTRACT Recent advances in atomic force microscopy (AFM) have enabled researchers to obtain images of supercoiled DNAs deposited on mica surfaces in buffered aqueous milieux. Confining a supercoiled DNA to a plane greatly restricts its configurational freedom, and could conceivably alter certain structural properties, such as its twist and writhe. A program that was originally written to perform Monte Carlo simulations of supercoiled DNAs in solution was modified to include a surface potential. This potential flattens the DNAs to simulate the effect of deposition on a surface. We have simulated transfers of a 3760-basepair supercoiled DNA from solution to a surface in both 161 and 10 mM ionic strength. In both cases, the geometric and thermodynamic properties of the supercoiled DNAs on the surface differ significantly from the corresponding quantities in solution. At 161 mM ionic strength, the writhe/twist ratio is 1.20–1.33 times larger for DNAs on the surface than for DNAs in solution and significant differences in the radii of gyration are also observed. Simulated surface structures in 161 mM ionic strength closely resemble those observed by AFM. Simulated surface structures in 10 mM ionic strength are similar to a minority of the structures observed by AFM, but differ from the majority of such structures for unknown reasons. In 161 mM ionic strength, the internal energy (excluding the surface potential) decreases substantially as the DNA is confined to the surface. Evidently, supercoiled DNAs in solution are typically deformed farther from the minimum energy configuration than are the corresponding surface-confined DNAs. Nevertheless, the work (ΔA_{int}) done on the internal coordinates, which include uniform rotations at constant configuration, during the transfer is positive and 2.6-fold larger than the decrease in internal energy. The corresponding entropy change is negative, and its contribution to ΔA_{int} is positive and exceeds the decrease in internal energy by 3.6 fold. The work done on the internal coordinates during the solution-to-surface transfer is directed primarily toward reducing their entropy. Evidently, the number of configurations available to the more deformed solution DNA is vastly greater than for the less deformed surface-confined DNA.

INTRODUCTION

A three-dimensional image of the path of a supercoiled DNA provides a complete account of its tertiary structure, from which fundamental topological and geometrical properties can be determined. Such properties include writhe, knot type, kind of supercoiling (interwound versus toroidal), number of interwound branches, pair correlation functions for subunits with particular contour separations, total pair correlation functions for all subunits with contour separations that exceed some minimum threshold value, radius of gyration (inertial) tensor, and structure factors for a range of scattering vectors. When the linking difference of a particular topoisomer is also known, then knowledge of the writhe also allows a determination of the net twisting strain, $\Delta t = t - l_0$, where t is the net twist, $l_0 = N\phi_0$ is the intrinsic twist, N is the number of basepairs, and ϕ_0 is the intrinsic (twist) succession angle of the unstrained DNA. Although diffusion and sedimentation coefficients and light scattering structure factors depend on the tertiary structure of the DNA, and provide useful tests of known structural models, their relationship to specific structural features, apart from the radius of gyration and structure factor, is neither unique nor simple. Consequently, there is great interest in any method that can image the tertiary path of a supercoiled DNA. At present, there are only a few methods capable of resolving such paths, namely conventional electron microscopy (EM), atomic force microscopy (AFM), scanning tunneling microscopy, and cryo-electron microscopy (cryo-EM). Except for cryo-EM, these methods all yield images of supercoiled DNAs that have been deposited on surfaces. In favorable cases, the desired structural features can be obtained for such surface-flattened supercoiled DNAs, but it is not known to what extent such properties differ from those of the corresponding species in solution.

For EM studies, a drop of DNA solution is typically deposited on a grid with some heavy metal stain and dried (Boles et al., 1990). EM images were analyzed in an attempt to infer certain properties of the supercoiled DNAs in solution, such as the writhe, writhe/twist ratio, and relative values of the bending and torsional rigidities (Ubbink and Odijk, 1999), but no account was taken of possible changes in structure when the DNA was transferred from solution to the imaging surface. For AFM studies, a drop of DNA solution is placed on a piece of mica (Rippe et al., 1997; Lyubchenko and Shlyakhtenko, 1997). There are several ways of "fixing" the DNA to the mica so that it can be imaged. Stable images have been obtained by pretreating the mica with a solution containing divalent cations such as Mg^{2+} ions (Bustamante et al., 1992; Vesenka et al., 1992; Hansma et al., 1992). Mica has also been chemically modified to make AP-mica by reacting the surface with 3-aminopropyltriethoxysilane followed by methylation of the amino group to form a quaternary amine, and then hydro-

Submitted July 18, 2001, and accepted for publication November 12, 2001.

Address reprint requests to Bryant S. Fujimoto, Dept. of Chemistry, Campus Box 351700, Univ. of Washington, Seattle, WA 98195-1700. Tel.: 206-543-4529; Fax: 206-685-8665; E-mail: fujimoto@u.washington.edu.

0006-3495/02/02/944/19 $2.00

lysis of the ethoxy groups (Lyubchenko et al., 1992, 1993; Lyubchenko and Shlyakhtenko, 1997). The reaction results in quaternary alkyl ammonium groups tethered to silicon atoms at the surface of the mica via propylene linkers. The interactions between the quaternary alkyl ammonium groups on the surface and the DNA are sufficient to confine the DNA to the surface, but not so strong as to completely immobilize the DNA, because the AFM images show signs of DNA motion during scanning. Native supercoiled DNAs deposited and imaged on AP-mica in 20 mM Tris-HCl, pH 7.6, 1 mM EDTA, with and without 160 mM NaCl provide perhaps the best examples of equilibrated surface structures under benign conditions (Lyubchenko and Shlyakhtenko, 1997). Until now there has been no attempt to model the structures observed.

Cryo-EM involves rapid supercooling of a thin film of DNA solution on a carbon grid. The hope is that vitrification occurs so rapidly that the supercoiled DNA is trapped in its solution configuration, which can then be visualized by electron microscopy. However, important discrepancies were found between cryo-EM and solution measurements on supercoiled plasmids. In particular, the significant increase in molecular extension and radius of gyration (R_g) upon increasing the ionic strength from ~5 to 100 mM that was seen in cryo-EM (Adrian et al., 1990; Bednar et al., 1994) was directly contradicted by solution measurements of R_g, which instead declined with increasing ionic strength over that same range (Gebe et al., 1996; Hammermann et al., 1998). Moreover, the cryo-EM structures of supercoiled DNAs in 100 mM ionic strength differed considerably from the solution structures predicted by Monte Carlo simulations, which, at the same time, predicted light scattering structure factors, diffusion coefficients, and supercoiling free energies in rather good agreement with experiments over a wide range of superhelix densities (Gebe et al., 1995, 1996). These discrepancies were tentatively ascribed to an artifact of the cryo-EM, specifically to an increase in intrinsic twist with decreasing temperature, which drives the writhe toward more negative values, and significant equilibration of the tertiary structures during the early stages of the cooling process. The rapid appearance of structures closely resembling those seen in cryo-EM in a −50°C simulation strongly supported this suggestion (Gebe et al., 1996).

The principal objectives of this Monte Carlo simulation study are 1) to assess the changes in tertiary structure as a supercoiled DNA is transferred from solution to the surface by gradually imposing a flattening potential, 2) to calculate and analyze the work done on the supercoiled DNA by the confining potential, and 3) to model both solution and surface structures in 161 and 10 mM ionic strength and to compare those with the reported AFM images (Lyubchenko and Shlyakhtenko, 1997).

Mesoscopic models of supercoiled DNAs have been simulated by Metropolis Monte Carlo methods (Vologodskii and Cozzarelli, 1994; Langowski et al., 1994; Gebe et al., 1995, 1996; Schurr et al., 1995; Gebe and Schurr, 1996; Heath et al., 1996a; Delrow et al., 1997a; Rybenkov et al., 1997a,b; Velichko et al., 1999, 2000; Podtelezhnikov et al., 1999) and by Brownian dynamics protocols (Chirico and Langowski, 1994; Heath et al., 1996b; Hammermann et al., 1997, 1998; Jian et al., 1998). Calculations to determine the minimum energy configurations have also been reported (Hao and Olson, 1989a,b,c; Fenley et al., 1994; Yang et al., 1995; Zhang et al., 1994; Swigon et al., 1998; Martino and Olson, 1998; Fain and Rudnick, 1999), but the resulting structures are not representative of those in finite temperature ensembles of supercoiled DNAs in solution (Sprous et al., 1996), as will be further demonstrated below.

Two previous simulations of the effects of surface confinement on the tertiary structures of supercoiled DNAs have been reported. In the first case, configurations were drawn from a simulated equilibrium ensemble of supercoiled DNAs in solution and placed in a one-dimensional harmonic potential (acting on the individual subunits), which acted to flatten the DNA (Vologodskii et al., 1992). Because the intent was to simulate relatively rapid, irreversible (nonequilibrium) flattening, no attempt was made to simulate the flattening process in a reversible (equilibrium) or nearly reversible manner, and the number of simulation moves was far too small for even approximate equilibration in the surface potential. In the second case, a relatively small (≤200 bp) circular DNA was simulated in the presence of a one-dimensional Leonard–Jones potential (Velichko et al., 2000). However, the other physical parameters of that model were not directly related to the known physical properties of the DNA, so the quantitative relevance of the results is uncertain. As far as we are aware, the present simulations are the first to assess possible changes in tertiary structure that accompany the equilibrium (or near equilibrium) transfer of a supercoiled DNA from solution to the surface, and also the first to investigate the work performed on the DNA by the surface potential.

Our program and algorithms for simulating supercoiled DNAs with isotropic bending potentials have already been described (Gebe et al., 1995). When supplied with appropriate input parameters, that program satisfactorily reproduced experimental values of the supercoiling free energy (Gebe et al., 1995), translational diffusion coefficient, and static structure factor of the same plasmid DNA over a wide range of superhelix density in 0.1 M ionic strength (Gebe et al., 1996). In view of this, we suggest that such simulations provide a satisfactory representation of the configurations present in solution. We are not attempting to model the details of any particular set of interactions between the DNA and the surface. Rather, we are analyzing only the effect of restricting the DNA to roughly planar configurations on various characteristics of its tertiary structure. A detailed comparison of our Monte Carlo simulation procedure with that of Vologodskii and co-workers (Vologodskii

et al., 1992; Vologodskii and Cozzarelli, 1994; Rybenkov et al., 1997a,b; Podtelezhnikov et al., 1999) was presented previously (Gebe et al., 1995).

Brownian dynamics is clearly the method of choice for any theoretical study of dynamical properties of large circular DNAs (Heath et al., 1996b; Hammermann et al., 1997, 1998; Jian et al., 1998). However, for the study of equilibrium properties of large circular DNAs, Monte Carlo simulation techniques can achieve the desired results at a substantially reduced computational cost.

SIMULATION PROTOCOL

Monte Carlo simulations of supercoiled DNAs in the presence of a surface potential were performed by an extension of procedures developed previously (Gebe et al., 1995, 1996; Schurr et al., 1995; Gebe and Schurr, 1996; Delrow et al., 1997a). The closed circular DNA is modeled as a string of N contiguous cylindrical subunits, each of length b. In this work, $N = 134$, and $b = 95.4$ Å, which corresponds to a total length of 3760 bp. This length is the same as that of the pSA509 plasmid studied by AFM (Lyubchenko and Shlyakhtenko, 1997). Hookean twisting and bending springs connect each subunit to it predecessor. The bending and twisting force constants are chosen to be uniform and to produce an equilibrium bending persistence length, $P = 500$ Å, and a torsional rigidity of $C = 2.1 \times 10^{-19}$ erg cm, which are typical values for plasmid DNAs under these conditions. Lyubchenko and Shlyakhtenko (1997) did not report the superhelix density or linking difference of their pSA509 DNA, so we have assumed a linking difference (Δl) of -17 turns in 161 mM ionic strength, which corresponds to a typical native superhelix density, $\sigma = -0.047$. The intrinsic twist is estimated to decrease by 1.6 turns when the ionic strength is decreased from 161 to 10 mM, hence, we assume also that $\Delta l = -15.4$ turns in 10 mM ionic strength. The temperature was set to 25°C.

In our previous work, the DNA was not subject to an external potential, so the position and orientation of the DNA in the laboratory frame were irrelevant. However, for simulations in the presence of a surface potential, it is necessary to track the position of the DNA in the laboratory frame and to allow the DNA to diffuse along the surface normal. Two different types of Monte Carlo moves are used. The first type (type 1) is essentially identical to that of our previous work and involves applying a small random rotation to every subunit in the chain. The second type (type 2) is a purely translational move at constant internal configuration and orientation. Only type 1 moves are generated during the solution simulations. For simulations in the presence of a surface potential, the program alternates between the two types of moves. In both cases, the number of Monte Carlo moves reported here is the number of type 1 moves attempted.

To generate a new trial configuration for the Monte Carlo simulation using a type 1 move, our simulation program generates a small random rotation for every subunit in the chain in the following manner, which uniformly samples the orientational configuration space of the chain (Gebe et al., 1995). For each subunit, we record the Euler angles that rotate a coordinate frame from coincidence with the laboratory frame to coincidence with the subunit frame. Then for each move, a set of small random rotations about each subunit's body-fixed x, y, and z axes is generated, and new Euler angles are calculated for each subunit. The maximum size of a rotation about any one of the subunit's body-fixed axes was typically 0.008 radians. A closure algorithm is then applied to enforce the constraint of circularity (Gebe et al., 1995). When calculating the positions of the subunits in the new trial configuration, one of the subunits is designated as subunit 1. The origin of subunit 1, which coincides with the tail of the first bond vector, remains fixed at the same laboratory coordinates as in the original configuration, and its laboratory coordinates are recorded. Any rotation of the entire DNA due to the small subunit rotations occurs around the origin of subunit 1. The designation of subunit 1 is shifted with each succeeding move to the next subunit in the chain, and the laboratory coordinates of the new subunit 1 are recorded. This new trial configuration is then tested to ensure that there are no excluded volume overlaps and that the chain has not become knotted. Then, the energy of the new trial configuration is calculated and the Metropolis criterion applied to decide whether the new trial configuration is to be accepted or rejected in favor of the original configuration.

To generate a new trial configuration for the Monte Carlo simulation using a type 2 move, our simulation program generates a small random displacement that is applied to the laboratory z-coordinate of subunit 1. The maximum size of this displacement will be discussed later. This new trial configuration has the same internal configuration as the original configuration, and so the internal energies of the two configurations are equal, and only the surface potential energies are different. The surface potential energy of the new trial configuration is calculated and the Metropolis criterion applied to decide whether the new trial configuration is to be accepted or rejected in favor of the original configuration.

The potential energy function

The reduced configuration energy of a particular configuration is defined by

$$E_{rc} = U_{el} + U_{bend} + U_{twist}^{min} + U_{surf}, \qquad (1)$$

wherein U_{el} is the inter-subunit potential energy and includes both the electrostatic and hard-cylinder interactions between different sections of the duplex DNA filament,

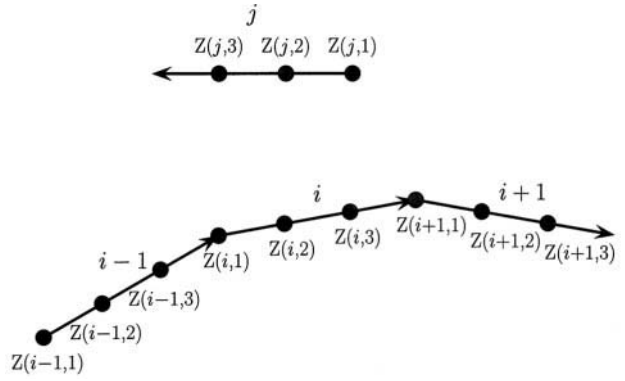

FIGURE 1 Schematic drawing of charge elements associated with each subunit. Each subunit has three charge elements evenly spaced along the bond between adjacent subunits. The nth subunit has charges $Z(n, 1)$, $Z(n, 2)$, and $Z(n, 3)$. In calculating the energy of the electrostatic repulsions between subunits that are not contiguous, (such as i and j), the electrostatic energy is summed for all possible pairs on elements associated with the two subunits. There are nine such interactions in this case. For adjacent subunits, (such as $i - 1$ and i) the charge element at the joint, $Z(i, 1)$, is not included, because the distance, and therefore the electrostatic potential energy, between $Z(i, 1)$ and any charge associated with subunit $i - 1$ is the same regardless of the configuration of the chain. There are only six interactions to be summed in this case. Similarly, for the electrostatic interactions between subunit i and subunit $i + 1$, $Z(i + 1, 1)$ is not considered, and there are only six interactions to be summed.

U_{bend} is the bending potential energy, and U_{surf} is the energy due to the surface potential, which holds the DNA close to a planar surface. $U_{\text{twist}}^{\text{min}}$ is the minimum twisting potential energy required for the molecule to have the correct total (or net) twist (Gebe et al., 1995, 1996). Two different intersubunit potentials have been used to calculate U_{el}, namely the screened Coulomb plus hard cylinder (SCPHC) potential, and the effective hard cylinder (EHC) potential.

For the SCPHC potential (Delrow et al., 1997a), the charge associated with each subunit is represented by three charge elements spaced 31.8 Å apart (see Fig. 1). The potential energy of interaction between two charge elements i and j on different subunits is

$$U_{\text{el}}^{\text{SCPHC}}(i, j) = U_{\text{HC}} + \frac{(Ze)^2}{\varepsilon}\left(\frac{e^{\kappa a}}{1 + \kappa a}\right)^2 \frac{e^{-\kappa r_{ij}}}{r_{ij}}. \qquad (2)$$

For the hard cylinder part of the potential, U_{HC}, the subunits are modeled as cylinders with a diameter $2a = 24$ Å. U_{HC} is infinite if the cylinders overlap, and zero otherwise. κ is the Debye screening parameter, e is the charge on an electron, $\varepsilon = 78.54$ is the relative dielectric constant of water, and r_{ij} is the distance between the ith and jth elements. The charge on an element, Z, is adjusted so that the potential from a string of identical contiguous elements in a linear array closely matches the solution of the nonlinear Poisson Boltzmann equation for an infinitely long cylinder with the same charge as DNA at all distances greater than $2a$ (Delrow et al., 1997a). To calculate the electrostatic energy of the supercoiled DNA, the distances between charge elements on all pairs of subunits are calculated. For those pairs of charge elements, where the distance is less than a certain cutoff distance specified below, the electrostatic energy is calculated using Eq. 2 and summed. Not included in the sum is any pair of elements whose separation distance is the same for all configurations. This includes any pair of charge elements on the same subunit, and any pair consisting of a charge element at the joint between two subunits and one on either of the two adjacent subunits (see Fig. 1). The cutoff distance was chosen to be sufficiently large that $U_{\text{el}}^{\text{SCHPC}}$ is negligible, in the sense that $U_{\text{el}}^{\text{SCHPC}}/kT < 7.3 \times 10^{-4}$ at the cutoff distance. In this study, two different ionic strengths were simulated, 161 mM ($Z = -16.7$ and $1/\kappa = 7.58$ Å, cutoff distance = 120 Å), and 10 mM, ($Z = -7.82$ and $1/\kappa = 30.4$ Å, cutoff distance = 240 Å).

The effective hard-cylinder diameter of the EHC potential is determined via Stigter's protocol using the full linear charge density of the DNA (Stigter, 1977; Delrow et al., 1997a). The subunits are simply considered to be hard cylinders, and any trial configurations that result in a cylinder overlap are discarded. For the work presented here, the equivalent hard cylinder diameter is 50 Å, which corresponds to an ionic strength of approximately 161 mM. Previous work suggests that $U_{\text{el}}^{\text{EHC}}$ is not as accurate as $U_{\text{el}}^{\text{SCPHC}}$ at low ionic strengths, so $U_{\text{el}}^{\text{EHC}}$ was not used for the simulations at 10 mM (Delrow et al., 1997a).

The bending potential energy (U_{bend}) between two adjacent subunits is $\frac{1}{2}\kappa_\beta\beta^2$, where β is the bending angle between adjacent subunits and κ_β is the force constant for the bending spring. The value of κ_β is adjusted so that the persistence length of the DNA is 500 Å. For the SCPHC potential, the value of the repulsive electrostatic energy (U_{el}) depends on the angle between adjacent subunits, which means that when the SCPHC potential is used for U_{el}, it contributes to the bending rigidity of the DNA and thus to its persistence length. Although the persistence length for all the DNAs simulated here is 500 Å, the actual value used for κ_β varies with the ionic strength and the model used to describe the inter-subunit potential energy. The procedure for determining κ_β is described in Appendix A.

The twisting potential energy ($U_{\text{twist}}^{\text{min}}$) is expressed in terms of the linking difference

$$\Delta l \equiv l - l_0 = t - l_0 + w, \qquad (3)$$

where l is the linking number of the DNA, w is the writhe of the configuration, t is the net twist, and $l_0 = N\phi_0$, where ϕ_0 is the intrinsic twist of a relaxed torsion spring. The topological constraint, $l = t + w$, has been used to obtain the right-hand side of Eq. 3. The (minimum) energy necessary to introduce a uniform twist, $\Delta t \equiv t - l_0 = \Delta l - w$, into the circular DNA is

$$U_{\text{twist}}^{\text{min}} = \frac{\alpha(2\pi)^2}{2N}(\Delta l - w)^2, \qquad (4)$$

where $\alpha = C/b$ is the force constant for the twisting springs between adjacent subunits. It was shown previously that fluctuations in the twisting strain of individual springs about their uniform average strain, $\Delta t/N$, can be neglected for the purpose of simulating either tertiary configurations or the supercoiling free energy, provided that both bending and intersubunit repulsive potentials are isotropic with respect to azimuthal rotation of the filament around its local symmetry axis (Gebe et al., 1995). In that case, such fluctuations in local twisting strain make always the same contribution to the configuration integral for every allowed trajectory of the helix axis (and its associated writhe) and for every value of the net twisting strain Δl. Hence, that contribution cancels out of all relative probabilities of observing any two tertiary configurations, and out of the reversible work of supercoiling. Because U_{surf} is similarly unaffected by the azimuthal rotation of the duplex around its local symmetry axis, fluctuations in local twisting strain still make the same contribution to the configuration integral for every allowed trajectory of the helix axis and for every value of Δl. In this case, too, that contribution of local twisting fluctuations cancels out of all relative probabilities of observing any two tertiary configurations, out of the reversible work of supercoiling, and out of the reversible work of transfer from "solution" to the "surface." When this contribution of local fluctuations about the mean twist is omitted, the residual energy function that appears in the configuration integral is called the reduced configuration energy, and is precisely that used here.

In addition to the internal potential energy of the supercoiled DNA, a surface potential energy (U_{surf}) is applied along the laboratory z axis to force the DNA to lie in the xy plane. The potential is applied to each subunit in the DNA, and takes the form

$$U_{\text{surf}}(z) = \begin{cases} (4.215 \times 10^{-31})z^{10} & \text{if} \quad z \le 0 \\ \lambda(1.829 \times 10^{-18})z^2 & \text{if} \quad z > 0 \end{cases}, \qquad (5)$$

where z is the position of the subunit in angstroms and λ is a constant that varies from 0 to 1 (to turn on the attractive part). For the purpose of calculating U_{surf}, the location of each subunit is taken to be at the joint between adjacent bond vectors. The value of the force constant for $z \le 0$ was chosen so that the potential energy for a single subunit equals kT at -50 Å (k is Boltzmann's constant) and has units of erg/Å^{10}. The value of the force constant for $z > 0$ was chosen so that, when $\lambda = 1$, the potential energy equals kT at 150 Å, and has units of erg/Å^2. The potential is plotted in Fig. 2 for three different values of λ. This is an ad hoc potential that hopefully reproduces certain features of the actual force field in the region around the potential minimum at $z = 0$, achieves a suitable degree of flattening of the DNA in the z direction normal to the surface, and allows equilibration of the surface-bound DNA within a reasonable simulation time. Particular features include the moderately

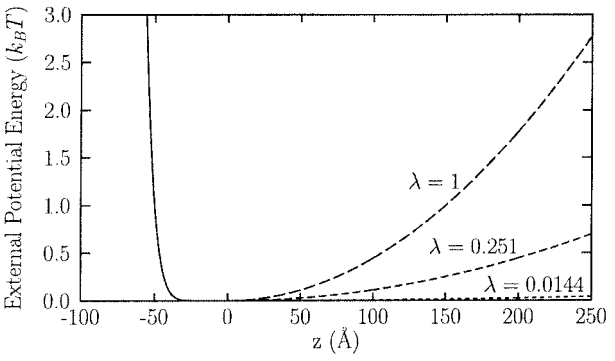

FIGURE 2 The external potential energy in units of kT. The solid line for $z < 0$ represents the surface against which the DNA is to be pushed. The potential for $z < 0$ is the same for all values of λ. The dashed lines are the potential energy for $z > 0$ plotted for three different values of λ. The simulated transfers start with $\lambda = 1.407 \times 10^{-5}$, and then, after equilibration, λ is increased in 10 steps to $\lambda = 1$.

hard wall ($U(z) \sim z^{10}$) for $z < 0$ inside the potential minimum, and a harmonic potential ($U(z) \sim z^2$) for $z > 0$ beyond the minimum, where the actual potential is expected to be not only harmonic near the minimum, but also much softer at any distance. The force constant of the hard wall potential for $z < 0$ was chosen to enable DNAs with the EHC potential to undergo some rearrangement (equilibration) by passing DNA sections over each other, even when pressed onto the surface with mean positions near $z \sim 0$. The force constant of the harmonic potential (when $\lambda = 1.0$) in the region $z > 0$ was chosen so that the mean z thickness in 161 mM ionic strength is about half the diameter of an unperturbed interwound superhelix. At that point, the induced deformation is already quite substantial. A practical consideration is that any significant increase in this harmonic force constant would not only increase the degree of flattening, but would also greatly slow the equilibration process, and prohibitively increase the required simulation time. In any case, AFM data discussed below suggest that, when the AFM tip is absent, the DNA strands are not everywhere pressed tightly onto the surface. This ad hoc potential provides a force field with suitable properties for our purposes, which are to assess the effects of equilibrium flattening on the geometric, topological, and thermodynamic properties associated with the internal coordinates of the DNA. However, the value of this surface potential at any particular z coordinate relative to that of the corresponding solution DNA is certainly incorrect, so that the total work of transfer from solution to the surface is also incorrect, and cannot be used to estimate the equilibrium constant for surface binding.

To simulate the transfer of a supercoiled DNA from solution to the surface, a circular chain of subunits with the desired superhelix density is first simulated in the absence of any surface potential ($U_{\text{surf}} = 0$). A configuration from that simulation is used as the initial configuration for a

simulation in a very weak surface potential ($\lambda = 1.407 \times 10^{-5}$, which, for any given subunit, equals kT at -50 Å and also at 40,000 Å). When this second simulation has equilibrated, then its final configuration is used as the first configuration of a third simulation, which uses a larger value of λ. This process is repeated, and, as λ is gradually increased in ten steps from $\lambda = 1.407 \times 10^{-5}$ to $\lambda = 1$, the supercoiled DNA is slowly pressed into relatively flat configurations. The eleven different values of λ for which simulations were performed as part of each transfer are: $\lambda = 1.407 \times 10^{-5}$, 5.625×10^{-5}, 2.250×10^{-4}, 9.000×10^{-4}, 3.600×10^{-3}, 1.440×10^{-2}, 4.5918×10^{-2}, 1.4062×10^{-1}, 2.500×10^{-1}, 5.102×10^{-1}, and 1.000. These eleven λ values correspond to eleven different z values at which $U_{surf} = k_B T$, which are as follows (in Å): 40,000, 20,000, 10,000, 5,000, 2,500, 1,250, 700, 400, 300, 210, 150. Of course, for all of these potentials, $U_{surf} = kT$ also at -50 Å. The maximum step size for type 2 (purely translational) Monte Carlo moves was 25 Å for $\lambda = 1.407 \times 10^{-5}$. As λ was increased, the maximum step size was decreased stepwise to 10 Å to ensure that at least 50% of the type 2 moves were accepted. This entire surface-transfer process is repeated for different initial configurations drawn from a Monte Carlo simulation in the absence of the surface potential. Results for the two inter-subunit potentials (U_{el}^{SCHPC} and U_{el}^{EHC}) at 161 mM ionic strength are compared to study the effect of our choice of inter-subunit potential on the observed configurations of the DNA. Simulations were also performed using U_{el}^{SCHPC} for an ionic strength of 10 mM to study the effect of ionic strength on the resulting configurations.

When $\lambda = 1.0$, the surface potential in Eq. 5 flattens the distribution of duplex DNA centers to a root-mean-squared (rms) thickness in the z direction of 47 Å in 161 mM ionic strength, and 57 Å in 10 mM ionic strength. In contrast, Lyubchenko and Shlyakhtenko (1997) reported a vertical image height of 17 ± 3 Å for single duplex strands, but performed no systematic AFM study of the height at points of duplex crossings. Such low heights imply that the z distribution of duplex centers has negligible thickness compared to the duplex diameter. This observation raises the question of whether the DNA is so greatly flattened by the surface potential alone, or instead adopts such structures only under the additional force of the AFM tip, which is operated in tapping mode. When the amplitude of tip oscillation is reduced, the apparent height of the DNA is observed to increase by as much as two-fold in some cases (Y. Lyubchenko, personal communication). This suggests that, under the reduced force associated with the reduced amplitude of the tip oscillation, the DNA may sometimes be encountered and detected at a height significantly above the surface. In any case, we did not extend our simulations to larger values of λ to achieve greater flattening for three reasons. 1) The rms thickness of the distribution of centers of the surface-confined DNA at $\lambda = 1.0$ is about half the diameter of a normal straight interwound superhelix in 161 mM ionic strength, so deformation of the superhelix "structure" is already considerable. 2) It is likely that the AFM tip in tapping mode drives some segments of the DNA that lie significantly "above" the surface down "onto" the surface. The somewhat smaller-than-expected observed vertical height of the flat-lying DNA in AFM images suggest that the force applied is sufficient to compress even the diameter of the duplex and/or the underlying surface. It would require considerably less force to drive high-lying DNA segments, including those atop a plectonemic helix, down onto the surface. For reasons discussed above, we suspect that, in the absence of additional tip force, some of the duplex segments probably lie significantly above the surface. 3) The rate of equilibration of surface-confined DNAs slows substantially with increasing λ, and any further increase in λ would require enormously longer simulations to reach equilibrium. Our DNAs are already sufficiently flattened that further forcing of one particular segment down onto the surface by an AFM tip is not likely to significantly rearrange the rest of the structure.

Last, we define the internal energy to be

$$E_{int} = E_{rc} - U_{surf}, \tag{6}$$

which is the reduced configuration energy of the internal coordinates of the supercoiled DNA.

Components of the radius of gyration tensor

During the simulation, configurations were typically saved once every 10,000 moves. These configurations were analyzed later to obtain the radius of gyration (R_g) and its components. R_g is defined by

$$R_g^2 = \left\langle \sum_{i=1}^{N} R_i^2/N \right\rangle, \tag{7}$$

where R_i is the distance from the center of mass of the molecule to the ith subunit. The components of the matrix of second moments is defined by

$$\mathbf{M} = \frac{1}{N} \begin{pmatrix} \sum_i x_i^2 & \sum_i x_i y_i & \sum_i x_i z_i \\ \sum_i x_i y_i & \sum_i y_i^2 & \sum_i y_i z_i \\ \sum_i x_i z_i & \sum_i y_i z_i & \sum_i z_i^2 \end{pmatrix}, \tag{8}$$

where the sum is over all the subunits in the configuration, and x_i, y_i, and z_i are the coordinates of the ith subunit in the center-of-mass coordinate system. This matrix can be calculated for each configuration. The trace of this matrix is R_g^2.

For comparison among solution and surface configurations, the matrix can be diagonalized, and the three diagonal components ordered to find the largest, second largest, and

smallest components of R_g. The largest component, $(R_g)_A$, is a measure of how elongated the configuration is. Due to the external potential, the z direction is different from the x and y directions. The zth diagonal element of the undiagonalized R_g matrix, $(R_g)_z$, is a measure of how thick the configurations are in the direction of the surface potential. In addition, the four elements of the upper left corner of the matrix can be diagonalized separately, to obtain the largest, $((R_g)_a)$, and smallest, $((R_g)_b)$ components of R_g in the laboratory xy plane. (We shall use upper case subscripts for R_g components when the full matrix is diagonalized and lower case subscripts when only the xy portion of the matrix is diagonalized.)

Other measures that were used to characterize the DNA include the inter-subunit correlation function, $g(r)$, and the distribution of distances of closest approach, $P(r)$. Both of these measures concern the distribution of distances between a subunit in the chain and other nonadjacent subunits. For the correlation function $g(r)$, if there is a subunit at the origin, then $4\pi r^2 g(r)\,dr$ is the probability that there is a subunit at a distance between r and $r + dr$. In calculating $g(r)$, subunits closer than 1200 Å in contour length (13 subunits) are omitted. The correlation function is normalized so that

$$4\pi \int_0^\infty g(r) r^2\, dr = 1. \tag{9}$$

The probability of closest approach, $P(r)\,dr$, is the probability that the closest subunit to a particular subunit lies at a distance between r and $r + dr$ away. In calculating this probability, subunits that are separated by less than 600 Å in contour length (7 subunits) are omitted.

Tests for equilibration

An important question is whether the simulation has reached equilibrium. The confining potential restricts the motions of the chain during the simulations, slowing its equilibration. Two different equilibration protocols were considered. In both protocols, we monitored the radius of gyration (R_g), because our previous experience has been that R_g equilibrates more slowly than other properties of the molecule, such as the writhe or the energy. For protocol A, the average value of R_g and the standard deviation of the population of R_g for each of two consecutive runs of 2.5–4 million moves were calculated. (The smaller number of moves was used for the smaller values of λ. With increasing λ, the number of moves for a given λ was increased because the fraction of Monte Carlo moves rejected due to excluded volume overlaps also increased.) The simulation was considered to have reached equilibrium for a given value of λ, if the average values of R_g for the two consecutive runs were within one standard deviation of each other. If this condition was not satisfied, additional simulations with the same value of λ were run until it was. Typically 8–12 million moves were necessary to equilibrate at each value of λ. Protocol B is the more demanding of the two. In that protocol, for a given value of λ, an equilibration simulation of 8–14 million moves was followed by two successive simulations of 3–4 million moves each. The configurations saved from each of the last two simulations were divided into five equal groups (first 20%, second 20%, etc.) and the average R_g was calculated for each group. The five values were then combined to obtain an average R_g and a standard deviation of the mean (s) for the penultimate ($R_g(1)$, $s(1)$) and final ($R_g(2)$, $s(2)$) simulations. The series of simulations at a given value of λ was considered to have reached equilibrium if $R_g(1)$ was in the range $R_g(2) \pm s(2)$ and $R_g(2)$ was in the range $R_g(1) \pm s(1)$. If this condition was not satisfied, then another set of three simulations (an equilibration simulation and two simulations to test equilibration) with the same value of λ were run until it was. Then λ was increased and the equilibration process repeated. Unless stated otherwise, this more demanding protocol was used for the results reported here.

Reversible work

The reversible work, or free energy, ΔA, required to transfer a DNA from solution (which for these purposes is approximated by the simulations with $\lambda = 1.407 \times 10^{-5}$) to the surface ($\lambda = 1$) is given by

$$\begin{aligned}\Delta A &= \int_{1.4\times10^{-5}}^{1} \left\langle \frac{\partial E_{rc}}{\partial \lambda} \right\rangle_\lambda d\lambda \\ &= \int_{1.4\times10^{-5}}^{1} \left\langle \frac{\partial U_{surf}}{\partial \lambda} \right\rangle_\lambda d\lambda \\ &= (1.829\times10^{-18}) \int_{1.4\times10^{-5}}^{1} \left\langle \sum_{i=1}^{N} z_i^2 \right\rangle_\lambda^+ d\lambda, \end{aligned} \tag{10}$$

where we have used the fact that E_{rc} depends on λ only through U_{surf}, and only through those subunits for which $z_i > 0$. The + superscript on the average in the last integral indicates that only subunits for which $z_i > 0$ are included in the sum. The average is calculated for each value of λ, and integrated numerically to yield ΔA. The reversible work calculated for surface confinement of the supercoiled DNA can be divided into two steps: the work to restrict the DNA to planar configurations (ΔA_{int}), and the work necessary to translate the center of mass of the DNA close to the surface (ΔA_{tr}). To calculate the reversible work associated with step 2, we take the final surface configuration from a transfer and treat it as a rigid array. Then the transfer is simulated again, while this rigid array is allowed to translate in the z direction

without undergoing either rotation or internal deformation. This procedure enables an estimate of the reversible work associated with step 2. The difference,

$$\Delta A_{\text{int}} = \Delta A - \Delta A_{\text{tr}}, \tag{11}$$

is an estimate of the reversible work of step 1. As discussed below, we can use the configurational work (ΔA_{int}) to obtain the change in the configurational entropy (ΔS_{int}) and show that the surface configurations compose a vanishingly small fraction of the configurations available to the DNA in solution. As noted above, the surface potential cannot account for all the contributions to the work, and so the total reversible work (ΔA) calculated here cannot be used to estimate adhesion strength or some similar property.

Computational details

All of the simulations using protocol C were run on the Chemistry Department Theoretical Chemistry Cluster, which, at this time, consists of IBM RS/6000 7043 Model 260 computers. The simulations using protocols A and B were run on a 350 MHz Pentium II-based computer, which uses Linux as its operating system, and on an earlier version of the Theoretical Chemistry Cluster, which, at that time, consisted of IBM RS/6000 Model 350 computers. The simulated transfers of the rigid arrays used to estimate the reversible work were run on University of Washington Uniform Access computers, which consist of IBM RS/6000 Model 370 computers.

We used the pseudo-random number generator RANLUXI (Hamilton and James, 1997), which was derived from the pseudo-random number generator RANLUX (Luscher, 1994; 1994, 1996). RANLUXI was used in its highest "luxury" (most chaotic) mode. It was checked here using some empirical tests described by Knuth (1981). Satisfactory results were obtained for the equidistribution (or frequency) test, the serial test (in two and three dimensions), the gap test, poker test, permutation test, runs test, max-of-5 test, collision test, and serial correlation test.

Two different graphics programs were used to view the configurations saved during the simulation. The first, glman (Faken and Jonsson, 1994), runs on an SGI R3000 Indigo, and was used for most of the visual inspection of the configurations. The second, Freyr, was installed on a Pentium III-based computer running Windows NT 4.0 and was used to generate the figures in this article. Freyr was written by Tung Le and Professor Hannes Jonsson and can be obtained by sending e-mail to hannes@u.washington.edu. In the figures, the DNA is drawn as a chain of cylinders, each 95.4 Å long and 24 Å in diameter. The configurations from the simulated transfer with nonzero λ also have a grid to represent the surface in the figure. The lines of the grid are drawn 1000 Å apart. In some of the figures, different parts of the chain are shaded differently to make it easier to see.

The transfer time

The very large number of simulation moves ($(200-600) \times 10^6$) required for the solution-to-surface transfers using protocol B raises the possibility that the time required for the DNA to undergo the simulated changes in tertiary structure might exceed the experimental surface deposition time. A time (Δt) can be associated with each Monte Carlo move by the formula (Gebe et al., 1996),

$$\Delta t = \frac{\langle \varepsilon^2 \rangle}{2D_{\text{r}}}, \tag{12}$$

where $\langle \varepsilon^2 \rangle$ is the mean squared angular displacement of a subunit around an axis perpendicular to its symmetry axis, and D_{r} is the rotational diffusion coefficient for end-over-end rotation of that subunit. For these simulations, ε is uniformly distributed on the interval $0 \le \varepsilon \le \varepsilon_0 = 0.008$ radian, hence $\langle \varepsilon^2 \rangle = \varepsilon_0^2/3 = 2.13 \times 10^{-5}$ radian^2. D_{r} is estimated from hydrodynamic theory for cylinders (Tirado and Garcia de la Torre, 1980). For a cylinder of length 95.4 Å and a radius of 12 Å, we obtain $D_{\text{r}} = 4.27 \times 10^{-5}$ s^{-1}. Combining these values in Eq. 12 yields $\Delta t = 3.7$ ps. Thus, the very longest simulation, 607×10^6 moves, corresponds to 2 ms. This time is an order of magnitude estimate of the time required by the molecule to undergo the changes in tertiary structure that we observe in our simulations. It is sufficiently short that the molecule could equilibrate in the surface potential well within the experimental surface deposition time.

RESULTS AND DISCUSSION

A total of 11 Monte Carlo simulations, each of which represents the transfer of a supercoiled DNA from solution to the surface, was performed. The DNA was modeled as a circular chain of 134 subunits, each 95.4 Å long, at a simulated temperature of 25°C. This DNA has 3760 bp, a persistence length of 500 Å, and a torsion constant between basepairs of 6.09×10^{-12} erg. The superhelix density was taken to be -0.0470 ($\Delta l = -17$) for simulations at 161 mM ionic strength and -0.0426 ($\Delta l = -15.4$) for simulations at 10 mM ionic strength. A list of the simulated transfers, giving the equilibration protocol, intersubunit potential energy function, and the number of moves in the simulated transfer is given in Table 1. Our choice of ionic strengths was intended to be similar to the two ionic strengths used by Lyubchenko and coworkers (Lyubchenko and Shlyakhtenko, 1997), and, as discussed below, we see some of the same changes in morphology observed by them. The actual ionic strength at the surface in the presence of the DNA is not known. Lyubchenko and coworkers give an upper

TABLE 1 List of simulated transfers

Simulated Transfer	Equilibration Procedure	Ionic Strength (mM)	Inter-subunit Potential	Moves in Simulation	Surface Configuration*
1	B	161	SCPHC	196,000,000	UI
2	B	161	SCPHC	518,000,000	3BI/UI
3	A	161	SCPHC	106,150,000	MBI
4	B	161	EHC	285,000,000	UI
5	B	161	EHC	607,000,000	3BI
6	A	161	EHC	51,000,000	3BI
7	A	161	EHC	82,800,000	3BI
8	A	161	EHC	72,000,000	MBI
9	B	10	SCPHC	442,000,000	UI
10	B	10	SCPHC	640,000,000	UI

*Predominant configuration during last two simulations with $\lambda = 1$. UI, unbranched interwound configuration; 3BI, three-arm branched interwound; 3BI/UI, first 75% are 3BI, then DNA converts to UI for the last 25% of simulation; MBI, multi-arm branched interwound.

bound for the surface density of AP moieties on the mica of 1/100 nm^2. They use this as an estimate of the surface charge density without taking account of any other charges on the surface of the mica, or the possibility that the AP moieties are not uniformly distributed. This is not sufficient to obtain the surface charge density directly beneath the surface-bound DNA, because all the charges on the surface must be included, and the possibility that the DNA is binding to clusters of AP moieties on the surface must be considered. Furthermore, even if the surface charge density were known, it is not clear that the ion distribution near the surface-confined DNA could be reliably estimated by the usual mean-field Poisson–Boltzmann theory, because correlation effects within the surface counterion cloud are known to be important for interactions between large charged objects in many cases. (Rouzina and Bloomfield, 1996; Grønbech-Jensen et al., 1997; Ha and Liu, 1997; Stevens, 1999; Menes et al., 2000)

161 mM ionic strength

Figure 3 *a* exhibits a typical simulated (protocol B) configuration of the supercoiled DNA with the SCPHC inter-subunit potential in solution ($\lambda = 0$) at an ionic strength of 161 mM. Average values of the different energies, the writhe, and the radius-of-gyration parameters are presented in Table 2. Also included in Table 2 are the corresponding quantities for simulations (protocol B) of solution DNAs with EHC inter-subunit potentials. Configurations such as that in Fig. 3 *a* were used as the starting configurations for transfers from solution ($\lambda = 0$) to surface ($\lambda = 1$) in 161 mM ionic strength. Figure 3 *b* displays a typical structure from a simulation (protocol B) of a surface-confined DNA ($\lambda = 1$) with the SCPHC inter-subunit potential in 161 mM ionic strength. Average values of the different energies, the writhe, and the radius-of-gyration parameters for surface-confined DNAs ($\lambda = 1$) with SCPHC potentials are included in Table 2 along with the corresponding quantities from simulations (protocol B) of surface-confined DNAs with the EHC inter-subunit potentials.

TABLE 2 Simulation results for DNAs in solution ($\lambda = 0$) and for the final simulation ($\lambda = 1$) in simulated transfers to the surface using protocol B and an ionic strength of 161 mM

	SCPHC		EHC	
	Solution $\lambda = 0$*	Surface Confined $\lambda = 1$†	Solution $\lambda = 0$‡	Surface Confined $\lambda = 1$§
Total Energy (erg $\times 10^{12}$)	7.40 ± 0.15	7.52 ± 0.12	7.31 ± 0.15	7.26 ± 0.05
Bending Energy (erg $\times 10^{12}$)	5.98 ± 0.12	5.43 ± 0.02	6.30 ± 0.13	5.65 ± 0.05
Twisting Energy (erg $\times 10^{12}$)	0.82 ± 0.02	0.64 ± 0.09	1.01 ± 0.07	0.69 ± 0.03
Electrostatic Energy (erg $\times 10^{12}$)	0.58 ± 0.01	0.59 ± 0.01	NA¶	NA¶
Surface Potential Energy (erg $\times 10^{12}$)	0	0.86 ± 0.004	0	0.91 ± 0.03
Internal Energy (erg $\times 10^{12}$)	7.40 ± 0.15	6.66 ± 0.12	7.31 ± 0.15	6.35 ± 0.06
Writhe	−11.98 ± 0.05	−12.60 ± 0.33	−11.43 ± 0.20	−12.37 ± 0.09
R_g (Å)	645 ± 78	1033 ± 25	641 ± 70	826 ± 39
$(R_g)_z$ (Å)‖	387 ± 85**	46 ± 0.5	397 ± 62††	47.5 ± 0.8
$(R_g)_A$ (Å)‡‡	529 ± 115	963 ± 29	524 ± 108	703 ± 25

*Averages from a solution simulation that used the SCPHC potential and was run in absence of any surface potential. The averages are for simulations totaling 68 million moves.

†Averages from the last two simulations in two different simulated transfers (4 million moves in each of 4 simulations, 16 million moves total).

‡Averages from a solution simulation that used the EHC potential and was run in absence of any surface potential. The averages are for simulations totaling 103 million moves.

§Averages from the last two simulations in two different simulated transfers (4 million moves in each of 4 simulations, 16 million moves total).

¶Not applicable for this simulation.

‖Component of the radius of gyration along the z axis, normal to the surface.

**This should be compared with the expected value if the simulation is rotationally averaged of $\sqrt{R_g^2/3} = 372$ Å.

††This should be compared with the expected value if the simulation is rotationally averaged of $\sqrt{R_g^2/3} = 370$ Å.

‡‡Largest component of the radius of gyration when the full second moment tensor is diagonalized.

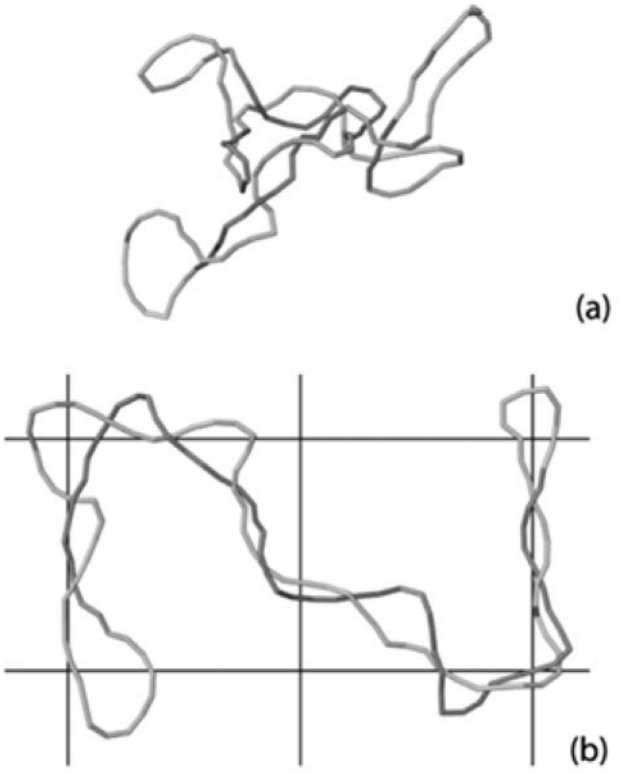

FIGURE 3 Configurations from simulations of a supercoiled DNA at 161 mM ionic strength. The simulated DNA is a chain of 134 subunits, each 95.4 Å long. The torsional rigidity is 2.1×10^{-19} erg cm, and the bending force constant was chosen to produce a persistence length of 500 Å. The electrostatic interactions were simulated using the SCPHC potential to simulate an ionic strength of 161 mM. The Debye screening length is 7.58 Å, and the charge on each charge element is −16.7 electrons. The chain is drawn as a contiguous chain of cylinders, each 95.4 Å long, and 24 Å in diameter. Sections of the chain are shaded differently to make it easier to see. (*a*) A solution ($\lambda = 0$) configuration of a supercoiled DNA. (*b*) A surface-confined ($\lambda = 1.0$) configuration of the same supercoiled DNA on approximately the same scale. This configuration is from simulated transfer 1. The lines are a grid drawn 1000 Å apart, and represent the surface underneath the DNA.

The types of surface configurations listed for each simulated transfer in Table 1 are the predominant configurations observed during the last two simulations with $\lambda = 1$. The values of R_g from these last two simulations were determined to have equilibrated according to the particular protocol used, which is also listed in Table 1. In 161 mM ionic strength, the two best equilibrated (protocol B) simulations with SCPHC potentials yielded mostly unbranched interwound (UI) configurations for surface-confined DNAs (cf. Fig. 3 *b*) in one case (simulated transfer 1), and approximately 75% three-arm branched interwound (BI) configurations and 25% UI configurations in the other (simulated transfer 2). It may be significant that the DNA in transfer 2 began the last two simulations in a three-arm BI configuration and then converted to a UI configuration and remained in a UI configuration through the end of the simulations with $\lambda = 1$. By comparison, the less equilibrated simulation (protocol A) yielded only multiarm BI configurations. The best-equilibrated (protocol B) simulations of surface-confined DNAs with EHC potentials yielded predominantly UI configurations in one case and only three-arm BI configurations in the other. However, two less well-equilibrated simulations (protocol A) using EHC potentials yielded only three-arm BI configurations and a third yielded only multi-arm BI configurations.

The question arises whether the surface-confined DNAs are capable of equilibrating among different configurations during simulations with $\lambda = 1$. This question can be addressed by monitoring the configuration of the surface-confined supercoiled DNAs during all of the simulations with $\lambda = 1$, rather than just the last two, which was done above to classify the equilibrated configuration. The total number of Monte Carlo moves simulated at $\lambda = 1$ was 39×10^6 for simulated transfer 1, 26×10^6 for transfer 2, 56×10^6 for transfer 4, and 26×10^6 for transfer 5. These simulations at $\lambda = 1$ were stopped when R_g was deemed to have equilibrated by the criterion of protocol B. In most cases, the configuration of the DNA evolved significantly during the $\lambda = 1$ simulations, which indicates that the supercoiled DNA was not locked into whatever configuration it had at the end of simulations with $\lambda = 0.5102$ (the penultimate value of λ). The evolution appeared to favor the conversion of branched configurations into unbranched configurations, but was not completely unidirectional.

For simulated transfer 1, the initial configuration for the $\lambda = 1$ simulation was a UI configuration, which included two loops extending away from the main axis of the DNA superhelix, one of which rotated to produce an additional crossover and thus an additional arm after approximately 230,000 moves at $\lambda = 1$. After this UI-to-BI conversion, which occurred at the beginning of the $\lambda = 1$ simulation for transfer 1, the supercoiled DNA remained in a three-arm BI configuration for approximately 23×10^6 moves before converting back to a UI configuration. No further BI configurations were observed during the 16×10^6 moves after converting back to a UI configuration.

For the other simulated transfers that used protocol B (2, 4, and 5) the initial configuration of the supercoiled DNA for the $\lambda = 1$ simulations was a three-arm BI configuration. During simulated transfer 2, the DNA remained in a three-arm BI configuration for the first 24×10^6 moves before converting to a UI configuration, where it remained for the last 2×10^6 moves of the simulation. During simulated transfer 5, the DNA remained in a three-arm BI configuration throughout. The only simulated transfer that exhibited repeated interconversions between UI and BI configurations was simulated transfer 4. In this case, the DNA adopted a three-arm or multi-arm BI configuration for the first 40.5×10^6 moves before converting to a UI configuration, and then over the next 7.5×10^6 moves it interconverted repeatedly between UI and three-arm BI configurations. The DNA then

converted back into a UI configuration where it remained for the last 8×10^6 moves of simulated transfer 4. The UI to three-arm BI conversions observed in transfer 4 involved a third branch that contained only a single crossover. The appearance of UI configurations by the end of 3 of the 4 best-equilibrated simulations suggests that the UI configuration might be preferred to some extent by surface-confined DNAs in 161 mM ionic strength, especially for the SCPHC potential. The observed interconversions between UI and BI configurations suggest that the DNA is capable of equilibrating among different surface configurations. The results for surface-confined DNAs with EHC potentials suggest either that BI configurations might be preferred in that case, or that equilibration has not been reached by most of those simulations, which is not unlikely for the three protocol A simulations.

Although the simulations appear to be at or close to equilibrium, the question arises whether the experimental surface-confined DNAs are also at equilibrium. In preliminary work, two transfers from solution were simulated using a rather small total number of moves in each case (17×10^6 vs. $50-640 \times 10^6$ in protocol B). Both of these simulations yielded tangled multi-arm structures which do not resemble the AFM images, but do resemble solution structures that have been instantaneously collapsed into two-dimensions. In a qualitative sense, the agreement between simulated and observed structures generally improved with increasing length, and equilibration, of the simulations. These finding suggest that the experimental surface-confined DNAs are probably equilibrated.

The solution DNAs are all interwound, but are not so readily classified into the two simple categories, unbranched or branched, as are the surface-confined DNAs. The solution DNAs often exhibit loops or partial branches that do not properly belong in either category. Nevertheless, solution DNAs occasionally exhibit UI configurations, which will be compared to their surface-confined counterparts subsequently.

Comparison of simulations with experiments at 161 mM ionic strength

Our simulated surface-confined supercoiled DNAs qualitatively resemble those observed in AFM studies (Lyubchenko and Shlyakhtenko, 1997). Of the eight simulated transfers using both protocols A and B, three exhibit terminal UI configurations, three exhibit terminal three-arm BI configurations, and two exhibit terminal multi-arm BI configurations. AFM images of supercoiled pSA509 (3760 bp) deposited from a solution containing 160 mM NaCl (plus 20 mM Tris-HCl, 1 mM EDTA, pH 7.6) displayed mostly UI and 3-arm BI configurations (cf. Fig. 2 of Lyubchenko and Shlyakhtenko, 1997). Although it is not possible to unambiguously count the number of crossovers in those AFM images, plausible estimates are in the range 10–12. In fact, the number of crossovers of our DNA in Fig. 3 *b* is 12, and the other surface-confined DNAs are similar. The ratio of average superhelix diameter to longest dimension, and the commonly low crossing angles of the simulated UI configurations, such as that in Fig. 3, appear to be roughly similar to those in the AFM images. Thus, to the extent that we are able to discern, the simulated surface-confined DNAs, especially those with the SCPHC potential, exhibit similar tertiary structures to those seen in AFM. However, as will be apparent from subsequent remarks, such AFM structures of surface-confined DNAs very likely differ from typical configurations of the same DNAs in solution.

The present mesoscopic model and simulation protocol with appropriate input parameters has achieved quantitative agreement with experimental supercoiling free energies, translational diffusion coefficients, and static structure factors of solution DNAs over a wide range of superhelix density in 100 mM ionic strength (Gebe et al., 1995, 1996), and is here found to achieve substantial agreement with AFM structures of surface-confined DNAs in 161 mM ionic strength. This inspires some confidence in the results for moderate ionic strengths.

Structural changes upon transfer to the surface

From Table 2, it seems that the mean writhe and radius-of-gyration parameters undergo significant alteration upon transfer from solution to the surface. In particular, for the SCPHC and EHC potentials, the writhe increases by 1.05- and 1.08-fold, respectively; R_g increases by 1.60- and 1.29-fold respectively; $(R_g)_A$ increases by 1.82- and 1.34-fold, respectively; and $(R_g)_z$ declines by factors of 0.125 and 0.128, respectively. The significant increase in the overall R_g arises from a considerable extension of the molecule in the *xy* plane, as manifested by the substantial increase in the largest eigenvalue, $(R_g)_A$, of the second moment matrix (Eq. 8), which far exceeds $(R_g)_z$. The process by which these changes occur is considered subsequently.

As a consequence of the 1.05-fold increase in writhe upon solution-to-surface transfer of the DNAs with the SCPHC potentials, the twist falls by a factor of 0.88 and the writhe/twist ratio increases by 1.20-fold. As a consequence of the 1.08-fold increase in writhe upon solution-to-surface transfer of the DNAs with the EHC potentials, the twist falls by a factor of 0.83 and the writhe/twist ratio increases by 1.33-fold. For either potential, these changes are significant. Ubbink and Odijk (1999) endeavored to infer the torsion elastic constant from the writhe/twist ratio of a solution DNA, which was assumed to be identical to that of its surface-deposited counterpart. It was also assumed that the solution DNAs exhibited a simple plectonemic helical structure and a bending rigidity corresponding to a persistence length of 500 Å. As already noted, in our simulations, the writhe/twist ratio is 1.20- to 1.33-fold greater for the surface-confined DNA than for the solution DNA, so use of the

TABLE 3 Properties of unbranched interwound configurations in solution (λ = 0, 161 mM)*

Intersubunit Potential	SCPHC	SCPHC	EHC
Number of Simulated moves while Unbranched Interwound	2.94×10^6	2.56×10^6	9.96×10^5
Internal Energy (erg $\times 10^{12}$)†	7.04 ± 0.15	7.20 ± 0.13	7.36 ± 0.28
Bending Energy (erg $\times 10^{12}$)	5.67 ± 0.15	5.74 ± 0.14	6.29 ± 0.38
Twisting Energy (erg $\times 10^{12}$)	0.81 ± 0.09	0.89 ± 0.05	0.80 ± 0.14
Electrostatic Energy (erg $\times 10^{12}$)	0.56 ± 0.01	0.57 ± 0.02	NA‡
Writhe	-12.01 ± 0.29	-11.77 ± 0.14	-12.02 ± 0.43
R_g (Å)	800 ± 85	814 ± 73	779 ± 83
$(R_g)_A$ (Å)§	710 ± 92	725 ± 79	687 ± 76

*The three largest, continuous runs of UI configurations observed in simulations of supercoiled DNA in solution at 161 mM ionic strength.
†Because there is no external potential for the solution simulations, the total energy equals the internal energy.
‡Not applicable for this simulation.
§Largest component of the radius of gyration when the full second moment tensor is diagonalized.

surface-confined value would underestimate the net twist in solution, and overestimate the torsion elastic constant (resistance to twist). It is also noteworthy that the simulated solution DNAs are not generally simple plectonemic supercoiled helices. Although the simulated surface-confined DNAs exhibit UI configurations that might be modeled approximately by an average plectonemic helix, such structures do not correspond to those of the simulated solution DNAs.

Although UI configurations were occasionally observed in simulations of solution DNAs, they occurred much less commonly than BI configurations with three or more arms, or structures for which distinct arms could not be identified. Solution configurations were scanned using the glman program, and the UI configurations (not necessarily flat) were noted. A configuration was classified as UI, if it had only two distinct end loops and no side loops with significant writhe. Such UI configurations of solution DNAs comprised ~13% of the total for the SCPHC potential and ~1% of the total for the EHC potential. The question arises whether these UI structures of the solution DNAs differ significantly from the UI configurations of the surface-confined DNAs. Average values of the various energies, the writhe, and the radius-of-gyration parameters of the solution UI configurations from three different simulations (protocol B) are presented in Table 3, and should be compared with the corresponding values in Table 2. For both the SCPHC and EHC potentials, the radius-of-gyration parameters, R_g and $(R_g)_A$, of the solution UI structures lie approximately midway between the corresponding values for the surface-confined DNAs on one hand and the average solution DNAs (all configurations) on the other, and differ significantly from both. For the SCPHC potential, the internal energy and bending energy of the solution UI configurations also lie roughly equidistant from the corresponding values for the surface-confined and average solution DNAs. For the EHC potential, the twisting energy and writhe of the solution UI configurations also lie roughly equidistant from the corresponding values for the surface-confined and average solution DNAs. Thus, solution UI configurations actually resemble neither the surface-confined configurations nor the average solution configurations in regard to certain geometrical and energetic properties.

Changes in the energies upon transfer to the surface

As is evident from Table 2, the total energy, including the everywhere positive surface potential energy, is unchanged within statistical error upon transferring the DNA from solution to the surface for either the SCPHC or the EHC intersubunit potential in 161 mM ionic strength. However, the internal energy, which consists of all potential energies except the surface potential energy, decreases significantly upon transfer from solution to the surface. In other words, the prevalent surface configurations lie closer in energy to the minimum energy structure of the supercoiled DNA, and, in that sense, are deformed less far from the minimum energy configuration than are the prevalent configurations in solution. We shall return to this somewhat surprising result when the work (free energy) of solution-to-surface transfers is discussed below. Upon transfer to the surface, the bending energy falls by the factors 0.91 and 0.90 for the SCPHC and EHC potentials, respectively; the twisting energy falls by the factors 0.78 and 0.68, respectively; and the electrostatic potential energy of the SCPHC potential remains practically constant. The substantial reductions in twisting energy are a direct consequence of the decline in twist by the factors 0.88 and 0.83, respectively. (Note that $(0.88)^2 = 0.77$ and $(0.83)^2 = 0.69$, both very close to their respective twisting energy reduction factors, 0.78 and 0.68.)

The question arises whether the failure to find low energy surface configurations in solution is due to a kinetic bottleneck of some kind that hinders equilibration of our simulations of solution DNAs, until they are exposed to the surface-flattening potential. To test this possibility, simulations of solution DNAs were carried out beginning with surface-confined equilibrium structures for both SCPHC and EHC potentials. In both cases, the configurations evolved from a UI surface configuration to a multi-arm BI solution structure in less than 10^6 moves. This indicates that the low energy surface structures are not kinetically inaccessible in our simulations. They are simply not favored in solution for entropic reasons.

TABLE 4 Reversible work calculations

Simulated Transfer	Equilibration Protocol	Inter-subunit Potential	Ionic Strength (mM)	Reversible Work (erg $\times 10^{12}$) [kT]		
				ΔA_{total}	ΔA_{tr}	ΔA_{int}
1	B	SCPHC	161	3.233 [78.5]	1.136 [27.6]	2.097 [50.9]
2	B	SCPHC	161	3.203 [77.8]	1.383 [33.6]	1.820 [44.2]
3	A	SCPHC	161	3.635 [88.3]	1.183 [28.7]	2.452 [59.6]
4	B	EHC	161	3.465 [84.2]	1.390 [33.8]	2.075 [50.4]
5	B	EHC	161	3.473 [84.4]	1.066 [25.9]	2.407 [58.5]
6	A	EHC	161	3.599 [87.5]	1.215 [29.5]	2.384 [57.9]
7	A	EHC	161	3.628 [88.1]	1.239 [30.1]	2.389 [58.0]
8	A	EHC	161	3.784 [91.9]	1.069 [26.0]	2.715 [66.0]
9	B	SCPHC	10	4.280 [104]	1.397 [33.9]	2.883 [70.0]
10	B	SCPHC	10	4.191 [102]	1.937 [47.1]	2.254 [54.8]

The work of transfer from solution to surface

The calculated work to transfer each supercoiled DNA from solution ($\lambda = 1.4 \times 10^{-5}$) to the surface ($\lambda = 1.0$) for each of the ten simulated transfers is indicated in Table 4. For both the SCPHC and EHC potentials, the better equilibrated protocol B yields slightly, but significantly, lower work values than does the less well equilibrated protocol A, and this effect is somewhat greater for the SCPHC potential than for the EHC potential. In the sequel, we discuss only the results for protocol B. In 161 mM ionic strength, the work of transfer is approximately $\Delta A = 78\ kT$ for the SCPHC potential and approximately $\Delta A = 84\ kT$ for the EHC potential. That part of ΔA associated with rigid-configuration center-of-mass translation (ΔA_{tr}) is obtained from a second reversible work simulation, in which the final surface configuration is transferred at constant configuration and orientation from the solution ($\lambda = 1.4 \times 10^{-5}$) to the surface (or vice versa). The remaining part of ΔA, namely ΔA_{int}, is associated with changes in internal coordinates, including uniform rotations of the entire molecule, and is obtained from ΔA and ΔA_{tr} via Eq. 11. Both ΔA_{tr} and ΔA_{int} are not ensemble averages, but pertain to the single (terminal) configuration of each solution-to-surface transfer. Because both ΔA_{tr} and ΔA_{int} are expected to vary significantly with the particular terminal configuration adopted, we expect considerably greater variability among the ΔA_{tr} and ΔA_{int} values than among the ΔA values for each type of simulation, as observed in Table 4. The change in configurational entropy, ΔS_{int}, associated with changes in the internal coordinates, including uniform rotations, upon solution-to-surface transfer is given by

$$\Delta S_{int} = (\Delta E_{int} - \Delta A_{int})/298. \quad (13)$$

Taking $\Delta A_{int} = 1.96 \times 10^{-12}$ erg as the average of the two values for the SCPHC potential, we obtain $(298)\Delta S_{int} = -2.70 \times 10^{-12}$ erg. Thus, the configurational entropic contribution to ΔA_{int} is negative and larger in magnitude than ΔA_{int} itself. The latter circumstance arises because ΔE_{int} is actually negative, as noted previously. Thus, in the process of transferring from solution to the surface, the supercoiled DNA proceeds downward in internal energy, but also in a sense much farther downward in internal configurational entropy, so that the $-298\Delta S_{int}$ term actually dominates ΔA_{int}. This implies that there are very many more configurations available with energies near the average energy of the solution DNA, than there are near the significantly lower average energy of the surface-confined DNA. Moreover, the states of the solution DNA are characterized by average properties that differ significantly from those of the less deformed surface-confined DNAs, as noted above. Thus, supercoiled DNAs in solution spend most of their time in a myriad of somewhat deformed higher energy configurations, but, when confined by the surface potential, spend most of their time in a much smaller number of somewhat less deformed lower energy configurations.

Strictly speaking, the quantity E_{int} in Eq. 13 is a potential-of-mean-force, rather than a simple potential energy, because it contains the quantity U_{twist}^{min}, which is known to be a temperature-dependent potential-of-mean-force that contains both energetic and entropic components (Delrow et al., 1997b, 1998; Schurr et al., 1997). For plasmid DNAs, the torsional rigidity decreases with increasing temperature, and this decrease accounts in large part for the observed decline of the supercoiling free energy with increasing temperature, and implies that a positive entropy change accompanies any increase in deformation of such torsion springs. Consequently, the decrease in twisting potential-of-mean-force and extent of deformation upon solution-to-surface transfer necessarily gives rise to an additional negative contribution to the total internal entropy changes (beyond the decrease in configurational entropy), which is implicitly included in $E_{int}/298$ in Eq. 13.

The process by which simulated surface confinement takes place

The process of simulated surface confinement of a supercoiled DNA in 161 mM ionic strength can be divided roughly into three stages. The boundaries of the three stages, which are only approximate (and not exactly the same for all transfers), are: stage I ($1.4 \times 10^{-5} \leq \lambda \leq$

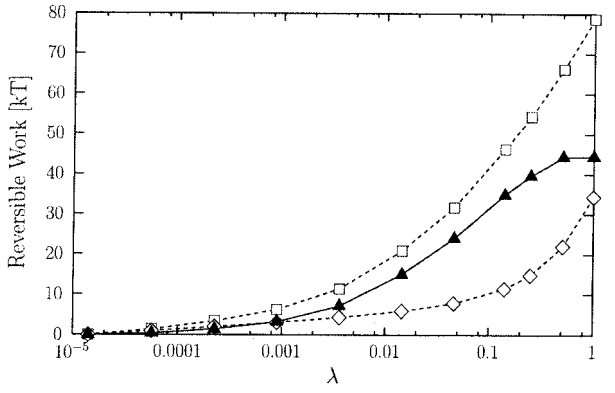

FIGURE 4 Reversible work as a function of λ for simulated transfer 2. The ordinate is the amount of reversible work done on the system as the DNA is transferred from a potential with $\lambda = 1.407 \times 10^{-5}$, to a potential with the λ indicated on the abscissa. (□) total reversible work; (◇) reversible work of *z*-translation; (▲) reversible work done on the internal coordinates of DNA, including its uniform rotation.

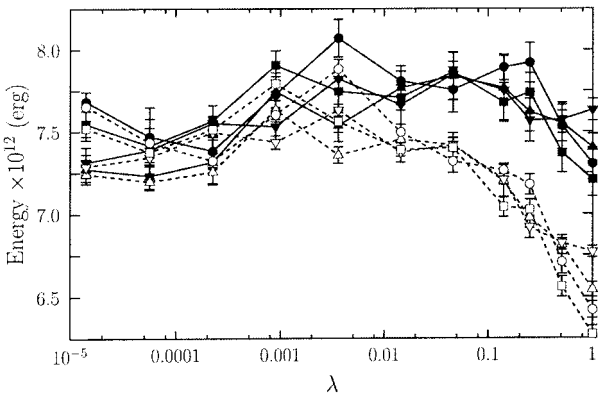

FIGURE 6 Total and internal energies versus λ for simulated transfers 1, 2, 4, and 5 (ionic strength = 161 mM, protocol B). The solid symbols are the total energies of the DNA, and the open symbols are the internal energies of the DNA. (▲, △) simulated transfer 1 (SCPHC); (▼, ▽) simulated transfer 2 (SCPHC); (■, □) simulated transfer 4 (EHC); (●, ○) simulated transfer 5 (EHC).

0.001); stage II ($0.001 \leq \lambda \leq 0.3$); and stage III ($0.3 \leq \lambda \leq 1.000$). In Fig. 4, ΔA, ΔA_{int}, and ΔA_{tr} are plotted versus λ (where λ is now the upper limit of the numerical integration in Eq. 10) for simulated transfer 2 in Table 1. The other transfers show very similar behavior. In stage I, the total reversible work performed on the DNA is divided more or less evenly between ΔA_{int}, and ΔA_{tr}. However, in stage II, the work is directly primarily into ΔA_{int}, and in stage III it is directed primarily into ΔA_{tr}. To understand what is happening here, it is helpful to examine the behavior of R_g, $(R_g)_z$ and the two principle components, $(R_g)_a$ (largest) and $(R_g)_b$ (smallest), of the second moment tensor in the *xy* plane perpendicular to *z*, which are displayed in Fig. 5. Throughout stage I, R_g and $(R_g)_a$ remain nearly constant, whereas $(R_g)_z$ exceeds $(R_g)_b$, but declines with increasing λ toward that value. At the smallest value of λ, the surface potential has practically no effect to either orient or compress the DNA, so we expect that all axes are equivalent, and $(R_g)_z = R_g/\sqrt{3} = (R_g)_x = (R_g)_y$, which is confirmed for $(R_g)_z$ in Fig. 5. When the second moment matrix in the *xy* plane is diagonalized, we expect $(R_g)_a > (R_g)_z > (R_g)_b$, as observed. As λ increases, the internal energies change relatively little in stage I, as shown in Fig. 6. The observed decrease in $(R_g)_z$ down to $(R_g)_b$ together with the near invariance of R_g, $(R_g)_a$ and the internal energy suggest that the molecule is being reoriented at approximately constant configuration during stage I, to align the smallest principal component of its second moment tensor along *z*. During stage II, $(R_g)_z$ continues to decrease, now below $(R_g)_b$, which remains relatively constant, whereas R_g and $(R_g)_a$ begin to increase significantly. During this stage, much more work is directed into ΔA_{int} than into ΔA_{tr}, even though the latter continues to grow. A significant decrease in internal energy also occurs during stage II, as shown in Fig. 6. These changes suggest that, during stage II, the molecule is being compressed in the *z* direction while extending primarily in one direction in the *xy* plane, and is thereby being driven into lower energy states by a substantial reduction in internal configurational entropy, which requires considerable work beyond ΔA_{tr}. In stage III, R_g, $(R_g)_a$, and $(R_g)_b$ remain relatively constant, whereas $(R_g)_z$ continues its slow decrease and the internal energy continues to decline. However, in stage III, the work of transfer is directed primarily into ΔA_{tr}, rather than ΔA_{int}. These observations suggest that the dominant process in stage III is progressive confinement and flattening by the surface potential at roughly constant configuration in the *xy* plane.

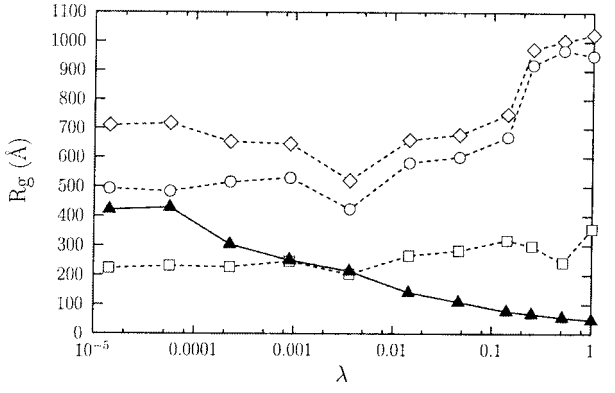

FIGURE 5 R_g and its components as a function of λ for simulated transfer 2. (◇) R_g; (○) $(R_g)_a$, the largest component of R_g in the *xy* plane; (□) $(R_g)_b$, the smallest component of R_g in the *xy* plane; (▲) $(R_g)_z$, the *z* component of R_g.

10 mM ionic strength

Figure 7 *a* exhibits a typical simulated (protocol B) configuration of the supercoiled DNA with the SCPHC intersub-

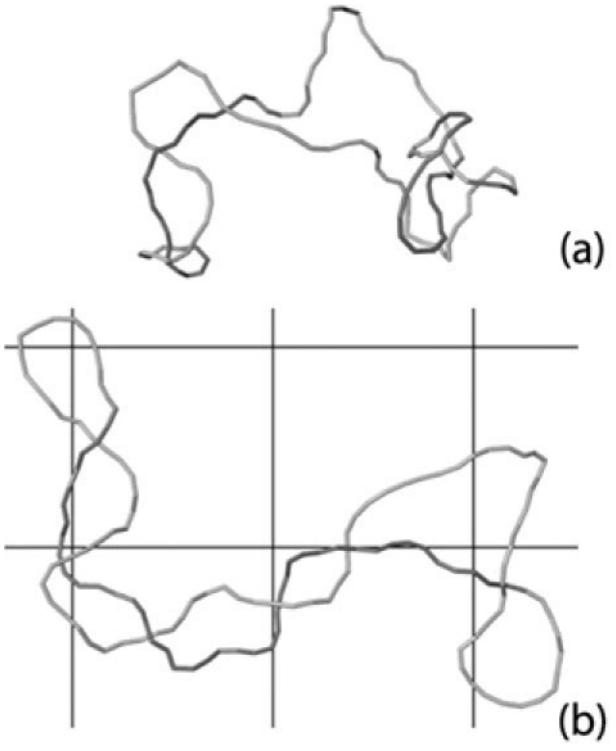

FIGURE 7 Configurations from simulations of a supercoiled DNA at 10 mM ionic strength. The simulated DNA is a chain of 134 subunits, each 95.4 Å long. The torsional rigidity is 2.1×10^{-19} erg cm, and the bending force constant was chosen to produce a persistence length of 500 Å. The electrostatic interactions were simulated using the SCPHC potential to simulate an ionic strength of 10 mM. The Debye length is 30.4 Å, and the charge on each charge element is −7.82 electrons. The chain is drawn as a contiguous chain of cylinders, each 95.4 Å long, and 24 Å in diameter. Sections of the chain are shaded differently to make it easier to see. (*a*) A solution ($\lambda = 0$) configuration of a supercoiled DNA. (*b*) A surface-confined ($\lambda = 1.0$) configuration of the same supercoiled DNA on approximately the same scale. This configuration is from simulated transfer 9. The lines are a grid drawn 1000 Å apart, and represent the surface underneath the DNA.

unit potential in solution ($\lambda = 0$) in 10 mM ionic strength, and Fig. 7 *b* displays a typical configuration from a simulation (protocol B) of a surface-confined DNA ($\lambda = 1.0$) with the SCPHC potential, also in 10 mM ionic strength. Average values of the different energies, the writhe, and radius-of-gyration parameters for both solution and surface-confined DNAs are presented in Table 5.

Both simulated transfers (9 and 10 in Table 1) yield predominantly UI configurations for the surface-confined DNAs in 10 mM ionic strength. Due to the decrease in linking difference from −17 to −15.4 turns, and the greater strength and range of the inter-subunit repulsions in 10 mM ionic strength, the simulated configurations of both the solution and surface-confined DNAs are much more open, and the writhe is considerably smaller than in 161 mM ionic strength. The smaller writhe in 10 mM ionic strength, as compared with that in 161 mM ionic strength, means that

TABLE 5 Simulation results for DNAs in solution ($\lambda = 0$) and for the final simulation ($\lambda = 1$) in simulated transfers using protocol C and an ionic strength of 10 mM

	SCPHC*	
	$\lambda = 0^{\dagger}$	$\lambda = 1^{\ddagger}$
Total Energy (erg × 10^{12})	17.19 ± 0.06	18.55 ± 0.02
Bending Energy (erg × 10^{12})	3.18 ± 0.01	2.87 ± 0.01
Twisting Energy (erg × 10^{12})	2.42 ± 0.06	2.61 ± 0.01
Electrostatic Energy (erg × 10^{12})	11.66 ± 0.01	11.78 ± 0.01
External Potential Energy (erg × 10^{12})	0	1.29 ± 0.01
Internal Energy (erg × 10^{12})	17.19 ± 0.06	17.26 ± 0.02
Writhe	−6.72 ± 0.10	−6.37 ± 0.02
R_g (Å)	709 ± 31	1026 ± 32
$(R_g)_z$ (Å)[§]	414 ± 62[¶]	57.2 ± 0.5
$(R_g)_A$ (Å)[‖]	597 ± 42	948 ± 49

*Only the SCPHC potential was used for the simulations at 10 mM ionic strength.
[†]Averages from solution simulation totaling 27 million moves.
[‡]Averages from the last two simulations run in simulated transfers 11 and 12 (4 million moves in each run, 16 million moves total).
[§]Component of the radius of gyration along the *z* axis.
[¶]This should be compared with the expected value if the simulation is rotationally averaged of $\sqrt{R_g^2/3} = 409$ Å.
[‖]Largest component of the radius of gyration when the full R_g matrix is diagonalized.

the contour length of surface-confined DNA between crossovers is larger in the former. These longer contour lengths between crossovers make it easier for the DNA to form a loop that could rotate to form a new crossover and thus an additional arm. As a result, short-lived UI to BI conversions were observed more frequently at 10 mM than at 161 mM.

Again the question arises whether the surface-confined DNAs are capable of equilibrating among different configurations during simulations with $\lambda = 1$. The total number of Monte Carlo moves simulated at $\lambda = 1$ was 62×10^6 for simulated transfer 9, and 78×10^6 for transfer 10. For simulated transfer 9, the initial configuration for the $\lambda = 1$ simulation was a multi-arm BI configuration, and for transfer 10, the initial configuration was a four-arm BI configuration. In both simulations, the DNA eventually converted to UI configurations. Simulated transfer 9 ended with a series of 18.6×10^6 moves in which the DNA was predominantly in UI. Simulated transfer 10 ended with a series of 8.6×10^6 moves in which the DNA was predominantly in UI configurations. In both cases, only 4% of configurations during these ending series of moves were three-arm BI configurations. The BI configurations observed during these ending series of moves were relatively short lived, persisting for less than 270,000 moves, and some cases less than 20,000 moves. The occurrence of the UI/BI conversions suggests that the DNA is capable of equilibrating among different surface configurations.

Solution structures were also checked for the occurrence of UI configurations, which occur even less frequently than in 161 mM ionic strength. In simulations totaling 67×10^6 moves, only about 100,000 UI configurations were found. The strong inter-subunit repulsions in this case evidently destabilize locally compact interwound helices in favor of more open structures with side loops.

Comparison of simulations with experiments at 10 mM ionic strength

The simulated structures of surface-confined DNAs resemble only two of the reported AFM configurations. They differ distinctly from the majority of AFM structures, which exhibit piled, or superposed, multiple-loop structures at one or more locations per molecule, where several strands cross at nearly the same point (Lyubchenko and Shlyakhtenko, 1997). These multi-strand crossing loci suggest some kind of very local intramolecular appregation, such as might be induced by a basic protein contaminant, or by a region of anomalously high positive charge density on the surface. In any event, our model, in which the surface potential is uniform and the inter-subunit potential is purely repulsive, appears to be incapable of generating such structures.

The two UI configurations seen in the AFM images both exhibit 6–7 crossovers at angles that are not far from 90°. The simulated UI configuration in Fig. 7 *b* exhibits six crossovers also at angles not far from 90°, and the other simulated configurations are similar. Thus, in regard to the minority UI configurations of the AFM images, agreement between the simulations and experiments in 10 mM ionic strength is satisfactory. The origins of the large discrepancy between the simulated configurations and the unusual majority structures of the AFM images in 10 mM ionic strength are unknown at this time.

The present mesoscopic model and simulation algorithm with the appropriate SCPHC potential for 10 mM ionic strength fails to predict surface-confined configurations that resemble the majority of structures seen in AFM. It also fails to predict either the substantial observed increase in R_g or the observed invariance of the translational diffusion coefficient of native supercoiled DNAs in solution, when the ionic strength is decreased from 100 to 10 mM. (Gebe et al., 1996; Hammermann et al., 1997, 1998; Rybenkov et al., 1997b; unpublished results) Given the considerable success of the model and simulation protocol in matching experimental data in 100 or 161 mM ionic strength, the lack of success in matching experimental data in 10 mM ionic strength strongly suggests that the model itself may be inadequate for the lower ionic strength. It is not unlikely that large-scale switching of the secondary conformation at ionic strengths $\leq$10 mM (Shibata et al., 1984; Wu et al., 1988, 1991; Wu and Schurr, 1989; Song et al., 1990; Naimushin et al., 2000), which has not been included in the model, may be required to account for some or all of the observed discrepancies.

Structural changes upon transfer to the surface

From Table 5, it is seen that the writhe and radius-of-gyration parameters undergo significant alteration upon transfer from solution to the surface. In particular, the writhe decreases by the factor 0.95; R_g increases by 1.45-fold; $(R_g)_A$ increases by 1.59-fold; and $(R_g)_z$ decreases by a factor of 0.14. The substantial increase in the overall R_g arises from a considerable extension of the molecule in the *xy* plane, which is manifested by the substantial increase in the largest eigenvalue of the second moment matrix (Eq. 8), which far exceeds $(R_g)_z$. As a consequence of the significant decrease in writhe upon solution-to-surface transfer, the twist increases by 1.04-fold, and the writhe/twist ratio decreases by the factor 0.91. In 10 mM ionic strength, the predicted changes in the writhe and writhe/twist ratio are in the opposite direction to, and significantly smaller than, the corresponding predicted changes in 161 mM ionic strength.

Changes in the energies upon transfer to the surface

Upon solution-to-surface transfer, the bending energy decreases significantly, but the twisting energy and the total energy increase significantly, and the internal energy remains almost unchanged. The 1.08-fold increase in twisting energy is directly attributable to the 1.04-fold increase in twist.

The work of transfer from solution to surface

The average work to transfer the DNA from solution to the surface in 10 mM ionic strength is $\Delta A = 103\ kT$ (cf. Table 4). The change in configurational entropy associated with changes in the internal coordinates is reckoned from the average ΔA_{int} and ΔE_{int} according to Eq. 11. Taking $\Delta A_{int} = 2.57 \times 10^{-12}$ erg as the average of the two values in Table 4, and $\Delta E_{int} \cong 0$ from Table 5, yields $(298)\Delta S_{int} = -2.57 \times 10^{-12}$ erg. In this case, ΔA_{int} consists almost entirely of configurational entropy, because $\Delta E_{int} \cong 0$. Here again, the work is directed primarily toward reducing the configurational entropy associated with the internal coordinates as the molecule becomes progressively trapped in the surface potential.

The process by which simulated surface confinement takes place

The process of simulated surface confinement in 10 mM ionic strength is similar in most respects to that in 161 mM ionic strength. It can be divided roughly into three stages, I, II, and III, as before. In Fig. 8, ΔA, ΔA_{int}, and ΔA_{tr} are plotted versus λ, and, in Fig. 9, R_g, $(R_g)_a$, $(R_g)_b$, and (R_z are

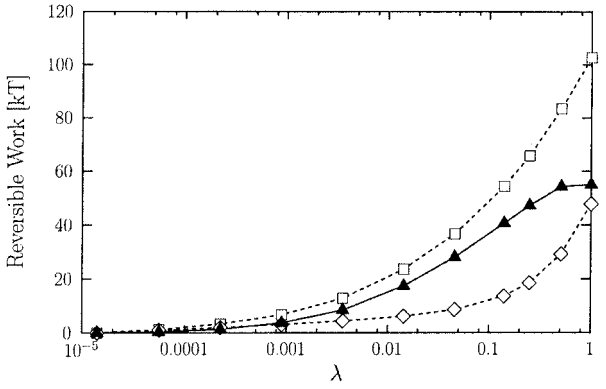

FIGURE 8 Reversible work as a function of λ for simulated transfer 13. The ordinate is the amount of reversible work done on the system as the DNA is transferred from a potential with $\lambda = 1.407 \times 10^{-5}$, to a potential with the λ indicated on the abscissa. (□) total reversible work; (◇) reversible work of *z*-translational; (▲) reversible work done on internal modes of DNA.

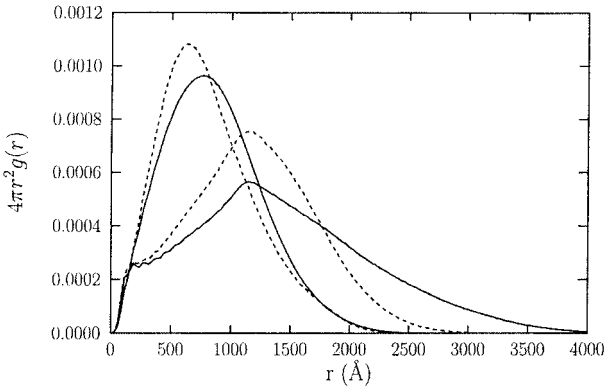

FIGURE 10 $4\pi r^2 g(r)$ versus r for two different values of λ (ionic strength = 161 mM). The solid lines are averages from simulated transfers 1 and 2 (SCPHC potential). The dashed lines are averages from simulated transfers 4 and 5 (EHC potential). The two different values of λ plotted are top to bottom, $\lambda = 0$ (solution) and $\lambda = 1$ (surface-confined).

plotted versus λ, all for transfer 10 in 10 mM ionic strength. Again, during stage I ($1.4 \times 10^{-5} \leq \lambda \leq 0.001$), the DNA is apparently reoriented at approximately constant configuration to align the smallest principal component of its second moment tensor along *z*. The bulk of the work is delivered during stage II ($0.001 \leq \lambda \leq 0.3$), and is directed predominantly into ΔA_{int}, which serves almost entirely to reduce the configurational entropy associated with the internal coordinates. Also during stage II, the molecule is compressed in the *z* direction while extending primarily in a single direction in the *xy* plane. Finally, during stage III ($0.3 \leq \lambda \leq 1.000$), the radius-of-gyration components remain relatively constant, and the work is directed primarily into ΔA_{tr} for progressive confinement and flattening at approximately constant configuration in the *xy* plane.

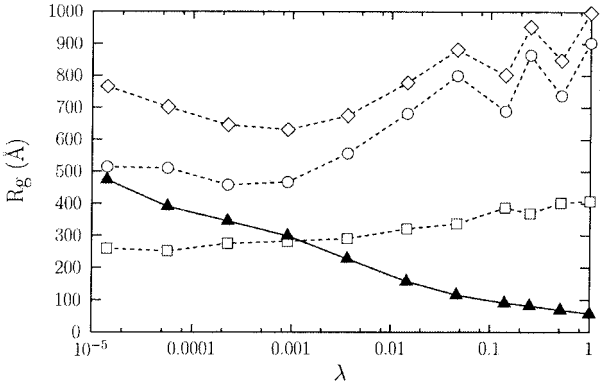

FIGURE 9 R_g and its components as a function of λ for simulated transfer 10. (◇) R_g; (○) $(R_g)_a$, the largest component of R_g in the *xy* plane; (□) $(R_g)_b$, the smallest component of R_g in the *xy* plane; (▲) $(R_g)_z$, the *z* component of R_g.

Comparison of SCPHC and EHC potentials in 161 mM ionic strength

In an earlier comparison of SCPHC and EHC inter-subunit potentials, simulations of a 1000-bp DNA were performed, and the two potentials yielded similar results for R_g, translational diffusion coefficients, and static structure factors, in 0.1 M NaCl, 1.0 M NaCl, and 0.1 M NaCl + 0.01 M $MgCl_2$. The present study allows us to compare the two potentials for a much larger DNA under both solution and surface-confined conditions, in 161 mM ionic strength. As can be seen in Table 2, the radius-of-gyration parameters are fairly similar for both potentials in the case of solution DNAs ($\lambda = 0$), but, for surface-confined DNAs ($\lambda = 1.0$), the SCPHC potential yields significantly larger R_g and $(R_g)_A$ values. An alternative way to compare the statistical structures associated with the two potentials is to examine radial distribution functions of the subunits. The quantity $4\pi r^2 g(r)$ is plotted versus *r* for DNAs with both potentials in solution ($\lambda = 0$), and also confined to a surface ($\lambda = 1.0$) in Fig. 10. In both environments, the distribution extends to larger distances for the SCPHC than for the EHC potential, and this difference is much greater for the surface-confined DNAs than for the solution DNAs. Another way to compare the statistical structures is to examine the distribution of nearest-neighbor distances, $P(r)$, which is plotted versus *r* in Fig. 11. The principal difference between the two potentials in regard to $P(r)$ occurs at the shortest distances, where the SCPHC potential allows much closer approaches.

Apart from its inadequacy at very short distances, the EHC potential yields results in reasonable accord with the supercoiled DNAs in solution, but not when they are surface confined. Thus, even in 161 mM ionic strength, the SCPHC potential should be used for surface-confined and perhaps also otherwise deformed supercoiled DNAs.

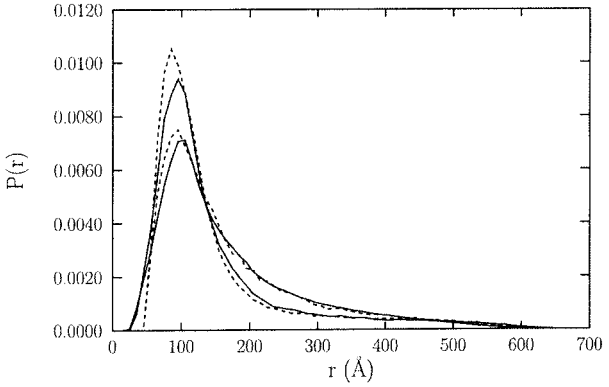

FIGURE 11 $P(r)$ versus r for two different values of λ (ionic strength = 161 mM). The solid lines are averages from simulated transfers 1 and 2 (SCPHC potential). The dashed lines are averages from simulated transfers 4 and 5 (EHC potential). The two different values of λ plotted are, top to bottom, $\lambda = 1$ (surface-confined), and $\lambda = 0$ (solution).

APPENDIX A

For the EHC potential, we use the procedure of Gebe et al. (1995) The bending force constant was chosen so that the persistence length (P) is 500 Å, when calculated according to

$$P = b/(1 - \langle \cos\,\theta \rangle),$$

where

$$\langle \cos\,\theta \rangle = \frac{\int_0^{\pi} d\theta \sin\,\theta \cos\,\theta \exp[-\kappa_\beta \theta^2/2k_B T]}{\int_0^{\pi} d\theta \sin\,\theta \exp[-\kappa_\beta \theta^2/2k_B T]},$$

and the integrals are evaluated numerically. This results in a bending force constant of $\kappa_\beta = 1.871 \times 10^{-13}$ erg.

For the SCPHC, the repulsive interactions between nearby subunits affect $\langle \cos\,\theta \rangle$. These interactions need to be included when determining κ_β. A trial value for κ_β was chosen, and simulations of linear chains of subunits were performed using the SCPHC. The subunit length, $b = 95.4$ Å, is the same as for the other simulations. The protocol is similar to the protocol for the simulation for circular DNAs, except that there is no twisting energy, the DNA is not constrained to be a closed circle, and there is no need to check for the molecule's knot type. $\langle \cos\,\theta \rangle$ is calculated from the simulation and the persistence length for that value of κ_β determined. For each value of κ_β, 20 simulations, each consisting of one million attempted moves, were performed. There were 10 simulations on chains of 10 subunits and 10 simulations on chains of 20 subunits. κ_β was adjusted until the $\langle \cos\,\theta \rangle$ for a set of simulations yielded an average persistence length of ~500 Å. For an ionic strength of 161 mM, $\kappa_\beta = 1.806 \times 10^{-13}$ erg, the 20 simulated persistence lengths were in the range 477–526 Å, with an average of 497 Å. For an ionic strength of 10 mM, $\kappa_\beta = 1.060 \times 10^{-13}$ erg, the 20 simulated persistence lengths were in the range 492–516 Å, with an average of 504 Å.

This work was supported in part by a grants R01-GM6185 from the National Institutes of Health and MCB-9982735 from the National Science Foundation.

REFERENCES

Adrian, M., B. ten Heggeler-Bordier, W. Wahli, A. Z. Stasiak, A. Stasiak, and J. Dubochet. 1990. Direct visualization of supercoiled DNA molecules in solution. *EMBO J.* 9:4551–4554.

Bednar, J., P. Furrer, A. Stasiak, J. Dubochet, E. H. Egelman, and A. D. Bates. 1994. The twist, writhe and overall shape of supercoiled DNA change during counterion-induced transition from a loosely to a tightly interwound superhelix. Possible implications for DNA structure in vivo. *J. Mol. Biol.* 235:825–847.

Boles, T. C., J. H. White, and N. R. Cozzarelli. 1990. Structure of plectonemically supercoiled DNA. *J. Mol. Biol.* 213:931–951.

Bustamante, C., J. Vesenka, C. L. Tang, W. Rees, M. Guthold, and R. Keller. 1992. Circular DNA molecules imaged in air by scanning force microscopy. *Biochemistry.* 31:22–26.

Chirico, G., and J. Langowski. 1994. Kinetics of DNA supercoiling studied by Brownian dynamics simulation. *Biopolymers.* 34:415–433.

Delrow, J. J., J. A. Gebe, and J. M. Schurr. 1997a. Comparison of hard-cylinder and screened Coulomb interactions in the modeling of supercoiled DNAs. *Biopolymers.* 42:455–470.

Delrow, J. J., P. J. Heath, B. S. Fujimoto, and J. M. Schurr. 1998. Effect of temperature on DNA secondary structure in the absence and presence of 0.5 M tetramethylammonium chloride. *Biopolymers.* 45:503–515.

Delrow, J. J., P. J. Heath, and J. M. Schurr. 1997b. On the origin of the temperature dependence of the supercoiling free energy. *Biophys. J.* 73:2688–2701.

Fain, B., and J. Rudnick. 1999. Conformations of closed DNA. *Phys. Rev. E.* 60:7239–7252.

Faken, D., and H. Jonsson. 1994. Systematic analysis of local atomic structure combined with 3D computer graphics. *Comp. Mat. Sci.* 2:279–286.

Fenley, M. O., W. K. Olson, I. Tobias, and G. S. Manning. 1994. Electrostatic effects in short superhelical DNA. *Biophys. Chem.* 50:255–271.

Gebe, J. A., S. A. Allison, J. B. Clendenning, and J. M. Schurr. 1995. Monte Carlo simulations of supercoiling free energies for unknotted and trefoil knotted DNAs. *Biophys. J.* 68:619–633.

Gebe, J. A., J. J. Delrow, P. J. Heath, B. S. Fujimoto, D. W. Stewart, and J. M. Schurr. 1996. Effects of Na^+ and Mg^{2+} on the structures of supercoiled DNAs: comparison of simulations with experiments. *J. Mol. Biol.* 262:105–128.

Gebe, J. A., and J. M. Schurr. 1996. Thermodynamics of the first transition in writhe of a small circular DNA by Monte Carlo simulation. *Biopolymers.* 38:493–503.

Grønbech-Jensen, N., R. J. Mashl, R. F. Bruinsma, and W. M. Gelbart. 1997. Counterion-induced attraction between rigid polyelectrolytes. *Phys. Rev. Lett.* 78:2477–2480.

Ha, B. Y., and A. J. Liu. 1997. Counterion-mediated attraction between two like-charged rods. *Phys. Rev. Lett.* 79:1289–1292.

Hamilton, K. G., and F. James. 1997. Acceleration of RANLUX. *Comput. Phys. Commun.* 101:241–248.

Hammermann, M., N. Brun, K. V. Klenin, R. May, K. Toth, and J. Langowski. 1998. Salt-dependent DNA superhelix diameter studied by small angle neutron scattering measurements and Monte Carlo simulations. *Biophys. J.* 75:3057–3063.

Hammermann, M., C. Steinmaier, H. Merlitz, U. Kapp, W. Waldeck, G. Chirico, and J. Langowski. 1997. Salt effects on the structure and internal dynamics of superhelical DNAs studied by light scattering and Brownian dynamics. *Biophys. J.* 73:2674–2687.

Hansma, H. G., J. Vesenka, C. Siegerist, G. Kelderman, H. Morrett, R. L. Sinsheimer, V. Elings, C. Bustamante, and P. K. Hansma. 1992. Reproducible imaging and dissection of plasmid DNA under liquid with the atomic force microscope. *Science.* 256:1180–1184.

Hao, M. H., and W. K. Olson. 1989a. Global equilibrium-configurations of supercoiled DNA. *Macromolecules.* 22:3292–3303.

Hao, M. H., and W. K. Olson. 1989b. Modeling DNA supercoils and knots with B-spline functions. *Biopolymers.* 28:873–900.

Hao, M. H., and W. K. Olson. 1989c. Molecular modeling and energy refinement of supercoiled DNA. *J. Biomol. Struct. Dyn.* 7:661–692.

Heath, P. J., J. B. Clendenning, B. S. Fujimoto, and J. M. Schurr. 1996a. Effect of bending strain on the torsion elastic constant of DNA. *J. Mol. Biol.* 260:718–730.

Heath, P. J., J. A. Gebe, S. A. Allison, and J. M. Schurr. 1996b. Comparison of analytical theory with Brownian dynamics simulations for small linear and circular DNAs. *Macromolecules.* 29:3583–3596.

James, F. 1994. RANLUX: a Fortran implementation of the high-quality pseudrorandom number generator of Luscher. *Comput. Phys. Commun.* 79:111–114.

James, F. 1996. RANLUX: a Fortran implementation of the high-quality pseudorandom number generator of Luscher [*Comput. Phys. Commun.* 1994, 79:111–114] (Erratum). *Comput. Phys. Commun.* 97:357.

Jian, H., T. Schlick, and A. Vologodskii. 1998. Internal motion of supercoiled DNA: Brownian dynamics simulations of site juxtaposition. *J. Mol. Biol.* 284:287–296.

Knuth, D. E. 1981. The Art of Computer Programming, 2nd ed., Vol. 2. Addison-Wesley Publishing Company, Reading, MA. 38–73.

Langowski, J., U. Kapp, K. Klenin, and A. Vologodskii. 1994. Solution structure and dynamics of DNA toposomers—dynamic light-scattering-studies and Monte-Carlo simulations. *Biopolymers.* 34:639–646.

Luscher, M. 1994. A portable high-quality random number generator for lattice field theory simulations. *Comput. Phys. Commun.* 79:100–110.

Lyubchenko, Y. L., A. A. Gall, L. S. Shlyakhtenko, R. E. Harrington, B. L. Jacobs, P. I. Oden, and S. M. Lindsay. 1992. Atomic force microscopy imaging of double stranded DNA and RNA. *J. Biomol. Struct. Dyn.* 10:589–606.

Lyubchenko, Y., L. Shlyakhtenko, R. Harrington, P. Oden, and S. Lindsay. 1993. Atomic force microscopy of long DNA: imaging in air and under water. *Proc. Natl. Acad. Sci. U.S.A.* 90:2137–2140.

Lyubchenko, Y. L., and L. S. Shlyakhtenko. 1997. Visualization of supercoiled DNA with atomic force microscopy in situ. *Proc. Natl. Acad. Sci. U.S.A.* 94:496–501.

Martino, J. A., and W. K. Olson. 1998. Modeling chain folding in protein-constrained circular DNA. *Biophys. J.* 74:2491–2500.

Menes, R., P. Pincus, and B. Stein. 2000. Charge fluctuations on membrane surfaces in water. *Phys. Rev. E.* 62:2981–2984.

Naimushin, A. N., B. S. Fujimoto, and J. M. Schurr. 2000. Dynamic bending rigidity of a 200-bp DNA in 4 mM ionic strength: a transient polarization grating study. *Biophys. J.* 78:1498–1518.

Podtelezhnikov, A. A., N. R. Cozzarelli, and A. V. Vologodskii. 1999. Equilibrium distributions of topological states in circular DNA: interplay of supercoiling and knotting. *Proc. Natl. Acad. Sci. U.S.A.* 96: 12974–12979.

Rippe, K., N. Mucke, and J. Langowski. 1997. Superhelix dimensions of a 1868 base pair plasmid determined by scanning force microscopy in air and in aqueous solution. *Nucl. Acids Res.* 25:1736–1744.

Rouzina, I., and V. A. Bloomfield. 1996. Macroion attraction due to electrostatic correlation between screening counterions. 1. Mobile surface-adsorbed ions and diffuse ion cloud. *J. Phys. Chem.* 100: 9977–9989.

Rybenkov, V. V., A. V. Vologodskii, and N. R. Cozzarelli. 1997a. The effect of ionic conditions on DNA helical repeat, effective diameter and free energy of supercoiling. *Nucl. Acids Res.* 25:1412–1418.

Rybenkov, V. V., A. V. Vologodskii, and N. R. Cozzarelli. 1997b. The effect of ionic conditions on the conformations of supercoiled DNA. I. Sedimentation analysis. *J. Mol. Biol.* 267:299–311.

Schurr, J. M., H. P. Babcock, and J. A. Gebe. 1995. Effect of anisotropy of the bending rigidity on the supercoiling free energy of small circular DNAs. *Biopolymers.* 36:633–641.

Schurr, J. M., J. J. Delrow, B. S. Fujimoto, and A. S. Benight. 1997. The question of long-range allosteric transitions in DNA. *Biopolymers.* 44: 283–308.

Shibata, J. H., J. Wilcoxon, J. M. Schurr, and V. Knauf. 1984. Structures and dynamics of a supercoiled DNA. *Biochemistry.* 23:1188–1194.

Song, L., B. S. Fujimoto, P. G. Wu, J. C. Thomas, J. H. Shibata, and J. M. Schurr. 1990. Evidence for allosteric transitions in secondary structure induced by superhelical stress. *J. Mol. Biol.* 214:307–326.

Sprous, D., R. K. Tan, and S. C. Harvey. 1996. Molecular modeling of closed circular DNA thermodynamic ensembles. *Biopolymers.* 39: 243–258.

Stevens, M. J. 1999. Bundle binding in polyelectrolyte solutions. *Phys. Rev. Lett.* 82:101–104.

Stigter, D. 1977. Interactions of highly charged colloidal cylinders with applications to double-stranded DNA. *Biopolymers.* 16:1435–1448.

Swigon, D., B. D. Coleman, and I. Tobias. 1998. The elastic rod model for DNA and its application to the tertiary structure of DNA minicircles in mononucleosomes. *Biophys. J.* 74:2515–2530.

Tirado, M. M., and J. Garcia de la Torre. 1980. Rotational dynamics of rigid symmetric top macromolecules. Application to circular cylinders. *J. Chem. Phys.* 73:1986–1993.

Ubbink, J., and T. Odijk. 1999. Electrostatic-undulatory theory of plectonemically supercoiled DNA. *Biophys. J.* 76:2502–2519.

Velichko, Y. S., K. Yoshikawa, and A. R. Khokhlov. 1999. Effect of twisting on the behavior of a double-stranded polymer chain: a Monte Carlo simulation. *J. Chem. Phys.* 111:9424–9433.

Velichko, Y. S., K. Yoshikawa, and A. R. Khokhlov. 2000. Surface-induced DNA superhelicity. *Biomacromolecules.* 1:459–465.

Vesenka, J., M. Guthold, C. L. Tang, D. Keller, E. Delaine, and C. Bustamante. 1992. Substrate preparation for reliable imaging of DNA molecules with the scanning force microscope. *Ultramicroscopy.* 42–44: 1243–1249.

Vologodskii, A. V., and N. R. Cozzarelli. 1994. Conformational and thermodynamic properties of supercoiled DNA. *Annu. Rev. Biophys. Biomol. Struct.* 23:609–643.

Vologodskii, A. V., S. D. Levene, K. V. Klenin, M. Frankkamenetskii, and N. R. Cozzarelli. 1992. Conformational and thermodynamic properties of supercoiled DNA. *J. Mol. Biol.* 227:1224–1243.

Wu, P., and J. M. Schurr. 1989. Effects of chloroquine on the torsional dynamics and rigidities of linear and supercoiled DNAs at low ionic strength. *Biopolymers.* 28:1695–1703.

Wu, P. G., B. S. Fujimoto, L. Song, and J. M. Schurr. 1991. Effect of ethidium on the torsion constants of linear and supercoiled DNAs. *Biophys. Chem.* 41:217–236.

Wu, P. G., L. Song, J. B. Clendenning, B. S. Fujimoto, A. S. Benight, and J. M. Schurr. 1988. Interaction of chloroquine with linear and supercoiled DNAs. Effect on the torsional dynamics, rigidity, and twist energy parameter. *Biochemistry.* 27:8128–8144.

Yang, Y., T. P. Westcott, S. C. Pedersen, I. Tobias, and W. K. Olson. 1995. Effects of localized bending on DNA supercoiling. *Trends Biochem. Sci.* 20:313–319.

Zhang, P., I. Tobias, and W. K. Olson. 1994. Computer simulation of protein-induced structural changes in closed circular DNA [published erratum appears in *J. Mol. Biol.* 1995 251:721]. *J. Mol. Biol.* 242: 271–290.